Eur. Phys. J. Plus (2018) **133**: 440
DOI 10.1140/epjp/i2018-12306-5

THE EUROPEAN PHYSICAL JOURNAL PLUS

Review

Resonances in neutron-induced reactions*

F. Gunsing[a]

CEA Irfu, University of Paris-Saclay, F-91191 Gif-sur-Yvette, France

Received: 3 June 2018 / Revised: 23 August 2018
Published online: 25 October 2018

Abstract. Resonances in neutron-induced reactions are important for reaction cross sections and nuclear data in general. They play a major role in nuclear technology for energy or medicine, but also in the study of nuclear level densities and stellar nucleosynthesis. An outline of the field of neutron physics is given, with a focus on neutron resonances, an introduction to the R-matrix formalism and the statistical behaviour of resonance observables.

1 Introduction

A remarkable feature of neutron-nucleus interactions is the resonance structure observed in the reaction cross sections at low incident neutron energies. These resonances in neutron-induced reactions result in variations of the cross section of several orders of magnitude over an energy range of as low as only a few electronvolt, depending on the nucleus. Resonances are also observed in proton-induced reactions near the Coulomb barrier, in particular for light nuclei. Since the electrically neutral neutron has no Coulomb barrier to overcome, and has a negligible interaction with the electrons in matter, it can directly penetrate and interact with the atomic nucleus, even at very low kinetic energies. The origin of the resonances is well understood and is related to the excitation of nuclear states in the compound nuclear system formed by the neutron and the target nucleus, at excitation energies lying above the neutron binding energy of typically several MeV.

The compound nucleus model was introduced by Bohr [1] to explain the observed resonances in neutron-nucleus reactions. In this model, a neutron incident on a nucleus gives rise to a sudden availability of an amount of energy corresponding to the neutron binding energy. This energy is rearranged among all nucleons which form a complex configuration corresponding to a defined, quasi-bound, nuclear state with an energy, spin and parity. Within Fermi's description of excitations of particle-hole configurations, such a state would correspond to an extremely complicated configuration of a many particle-many hole state. A typical life time of a compound nucleus is in the order of $\tau = \hbar/\Gamma \simeq 10^{-15}$ s, much larger than the typical time needed by a neutron to cross a nucleus without interaction, and also larger than direct reactions which are characterized by timescales of typically 10^{-22} s.

The type of interaction between neutrons and nuclei is largely dependent on the kinetic energy E of the neutron. The quantity that is most characteristic to illustrate this is the de Broglie wave length

$$\lambda = \frac{h}{\sqrt{2mE}} \tag{1}$$

of a freely moving neutron, where m is the neutron mass and h the Planck constant. To illustrate the scales of energy and wavelength, in fig. 1 the two quantities are shown on two corresponding scales, spanning the range of relevant neutron energies.

At very low neutron energies, typically below 0.1 eV, this wave length is of the order of the spacing between the atoms as they are structured inside a material. If the material has a crystalline structure, the neutron can be scattered from the lattice. This is commonly used in solid state investigation techniques like neutron diffraction and Bragg-edge transmission to determine the atomic and molecular structure in materials [2]. In this domain, neutron wavelengths

* Focus Point on "Rewriting Nuclear Physics Textbooks: Basic Nuclear Interactions and Their Link to Nuclear Processes in the Cosmos and on Earth" edited by N. Alamanos, C. Bertulani, A. Bonaccorso, A. Bracco, D. Brink, G. Casini, M. Taiuti.

[a] e-mail: gunsing@cea.fr

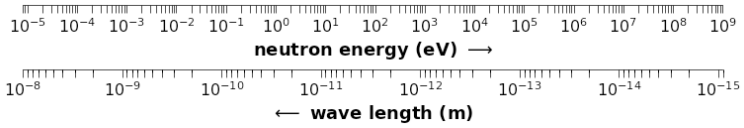

Fig. 1. The neutron kinetic energy scale and the corresponding de Broglie wavelength.

are used rather than kinetic energies. At higher energies the neutron interacts directly with the nucleus. Up to about 10 MeV, the wave length is comparable to the size of the nucleus. The main reaction mechanism in this region goes through compound nucleus formation and subsequent decay, which is discussed here. At still higher neutron energies, the wavelength becomes comparable to a single nucleon and the type of reactions that becomes dominant are direct reactions.

Neutron-induced nuclear reaction data are important for a number of research fields. In nuclear astrophysics, an intriguing topic is the understanding of the formation of the nuclei present in the universe and the origin of the chemical elements. Hydrogen and smaller amounts of He and Li were created in the early universe in the time period between about 100 seconds and 30 minutes after the Big Bang by primordial nucleosynthesis [3] after which galactic condensation and the formation of stars followed. Nuclear reactions in stars are at the origin of nearly all other nuclei. Nuclei up to the Fe-Ni region have been produced by nuclear fusion reactions in stars. Nearly all heavier nuclei beyond Fe were produced by neutron reactions, either during the He and C burning phases of stellar evolution [4–6], or at supernova explosions of massive stars [5,7] and in neutron star mergers [8]. Important input for stellar nucleosynthesis models are the neutron capture rates over a wide energy ranging from about 100 eV up to 1 MeV. For low stellar neutron densities as in the *s*-process, the neutron capture followed by beta-decay follows closely the valley of stability. The measurement of cross sections for many of those nuclei are within reach of current experimental facilities. In high neutron density-environments, like for the *r*-process, the reaction paths go far beyond stability and direct measurements of cross sections are not possible at present. Then the needed reaction rates for modelling tools, which are based on cross sections, beta-decay, nuclear masses and other quantities, depend entirely on nuclear model calculations. It must be noted that such models and systematics are always calibrated on experimental data.

Neutron-induced reaction cross sections also reveal the nuclear level structure in the vicinity of the neutron binding energy of nuclei [9–11]. The properties of these levels are crucial input to nuclear level density models [12–15]. Finally, neutron-induced reaction cross sections are a key ingredient for the safety and criticality assessment of nuclear technology, including research on medical applications [16], radiation dosimetry, the transmutation of nuclear waste, accelerator-driven systems, future reactor systems as in Generation IV, and nuclear fuel cycle investigations [17,18].

In fig. 2 the main reaction cross sections for a typical heavy nucleus are shown as a function of the energy. The reactions showing resolved resonances, typically elastic scattering, neutron capture, and for some nuclei fission, are clearly visible over a wide energy range. The position and extent of the resonance structure depend on the nucleus. Threshold reaction channels like (n, xn) or charged particle emission usually open up at higher energies. Also shown on the same energy scale in fig. 2 are several neutron energy spectra relevant for typical applications. The spectra are normalized to give the same height to stress the regions of interest. They correspond to a Maxwell-Boltzmann distribution of the neutron velocities. On the low-energy side the neutron flux of a theoretical spectrum of fully moderated neutrons is shown. For an infinite water moderator at a temperature of about 293.6 K, the neutron density of this thermal spectrum shows a maximum at a speed of 2200 m/s corresponding to an energy of 25.3 meV. On the high-energy side the idealised neutron distribution of thermal-neutron induced prompt fission neutrons from ^{235}U are shown.

Similar energy distributions are found for neutrons in certain stars where the synthesis of the nuclei heavier than about $A = 60$ takes place by neutron capture. For the *s*-process in Asymptotic Giant Branch stars, the neutrons originating mainly from $^{13}\mathrm{C}(\alpha, n)$ and $^{22}\mathrm{Ne}(\alpha, n)$ reactions, are present as a hot gas and with a Maxwellian kinetic energy distribution for temperatures with kT ranging from 5 to 100 keV.

Neutrons from fusion reactions, either from magnetic-confinement fusion with future applications of energy production or from inertial-confinement fusion have to be taken into account for issues related to shielding and activation. Reactions employed in most fusion developments are based on $\mathrm{D} + \mathrm{T} \rightarrow {}^4\mathrm{He} + n(14.1\,\mathrm{MeV})$ reactions (DT), as well as $\mathrm{D} + \mathrm{D} \rightarrow {}^3\mathrm{He} + n(2.5\,\mathrm{MeV})$ reactions (DD), which have quasi-mono-energetic energy spectra. Typical thermal fusion neutron spectra [19,20] at $T = 10$ keV are also shown in fig. 2.

The calculations and simulations for the various applications that need neutron-induced reaction data, can make use of evaluated nuclear data libraries. Examples of such libraries are JEFF in Europe [21], ENDF in the USA [22], JENDL in Japan [23], CENDL in China, BROND in Russia and several others. Neutron-induced reaction cross sections for resolved resonances are stored as *R*-matrix [24] resonance parameters which is the most concise and fundamental way to represent this type of cross sections, allowing to reconstruct cross sections at any temperature.

In the case of a beam of neutrons incident on target nuclei in a material at rest, the effect of the thermal motion of the target nuclei has an important broadening effect on the observed resonant cross section because of the spread

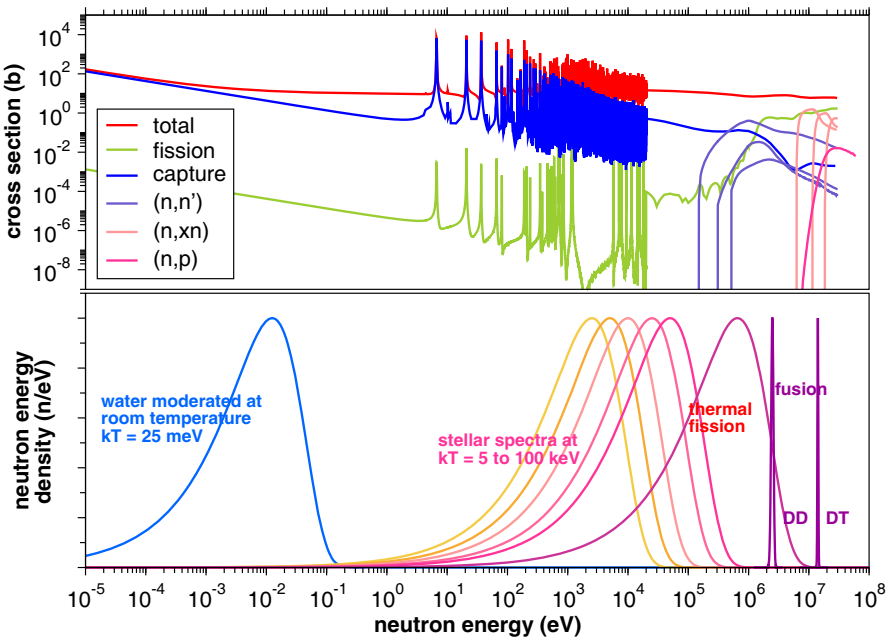

Fig. 2. Neutron-induced reaction cross sections for a typical heavy nucleus as a function of the neutron kinetic energy (upper panel), together with characteristic neutron energy distributions present in stellar environments and in technological applications like fission and fusion (lower panel). All distributions have been normalized to their maximum value.

in the velocity of the neutron. For metallic materials at temperature T, this movement can be described in a good approximation by the free gas model [25], resulting in a Gaussian broadening of the resonances with a standard deviation,

$$\sigma_D = \sqrt{\frac{2kT}{A}E}\,, \tag{2}$$

where the reduced mass in neutron-nucleus center of mass system is approximated by $1/A$. Since Doppler broadening is present in the interaction of neutrons incident on nuclei in a material, cross sections are often given as Doppler broadened at a specific temperature T.

Evaluated nuclear data libraries have started historically with a focus on nuclear technology applications, nowadays they are general purpose libraries intended to be universal. For nearly any nuclear data application and simulation code, the content of an evaluated nuclear data library is not directly useable but needs to be processed to extract the needed information in a suitable format. For example From these parameters a reaction cross section can be calculated with the appropriate thermal broadening needed for an application. This Doppler broadened cross section can then be merged with the energy range of smooth cross sections, and stored as interpolation tables, in order to obtain the reaction cross section over a wide energy range for a given temperature. Several special purpose libraries with derived quantities exist as well. For example the database KADoNiS [26] is dedicated to Maxwellian averaged capture cross sections relevant for stellar nucleosynthesis. It contains data both calculated from evaluated nuclear data libraries and from experiments. The EXFOR data base [27] is the international storage and retrieval system for experimental results. It contains data that are often not available in numerical form in publications and laboratory reports. Detailed results of measurements of neutron-induced reactions, for a large part originating from experiments using accelerators [28], are collected in EXFOR.

2 R-matrix for neutron-induced reactions

2.1 Scattering from a one-dimensional potential well

The nowadays standard way to describe the highly fluctuating cross sections in neutron-induced reactions is by means of the R-matrix formalism. Before going to an introduction of the R-matrix applied to neutron-nucleus reactions, intended for experimental physicists, we take a look at a simple quantum system to illustrate the basic idea of resonances. An instructive example introducing the idea of compound nucleus reactions is the 1-dimensional problem of scattering from a one-dimensional potential well for a spinless particle.

We can solve the time-independent Schrödinger equation,

$$-\frac{\hbar^2}{2m}\frac{\mathrm{d}^2\psi(x)}{\mathrm{d}x^2} + V(x)\psi(x) = E\psi(x), \tag{3}$$

for this system in order to find solutions for $\psi(x)$ and E. The full solution $\Psi(x,t) = \psi(x)\exp(-i\omega t)$ includes the time dependence with $\omega = E/\hbar$. There are many textbook examples in one dimension of potentials with a simple shape, dividing the space in a few simple geometric regions. The approach is solve the Schrödinger equation for each of the regions separately, which introduces integration constants that take values when the different regions are matched. These are the boundary conditions which are inherent to solving ordinary differential equations. At the boundaries of the potential, we require that the wave function $\psi(x)$ is continuous, and that the first derivative $\mathrm{d}\psi/\mathrm{d}x$ is continuous as well. Another requirement related to the probability density $\Psi^*\Psi$ is that $\psi(x)$ for bound states remains finite which give constraints for the solution in the limits to $\pm\infty$.

We consider a particle incident from the left with mass m and energy E that interacts with a square potential well $V(x)$ of depth $-V_0$ (V_0 is the absolute magnitude of the well, the minus sign indicates that we have a well instead of a barrier) when $-a < x < a$, and zero elsewhere. So there are three regions, numbered 1 ($x < -a$), 2 ($-a < x < a$) and 3 $x > a$.

We start looking for solutions for the bound states, so $E < 0$. The wave function must vanish for $x \to \pm\infty$. The general solutions for the bound states are therefore $\mathrm{d}\psi/\mathrm{d}x$

$$\psi_1(x) = A_1 e^{k_1 x}, \tag{4}$$

$$\psi_2(x) = A_2 e^{ik_2 x} + B_2 e^{-ik_2 x}, \tag{5}$$

$$\psi_3(x) = B_3 e^{-k_3 x}. \tag{6}$$

Requiring the continuity of both $\psi(x)$ and $\mathrm{d}\psi/\mathrm{d}x$ at the boundaries $x = -a$ and $x = a$ and taking into account that $k_1 = k_3$, give the following two sets of implicit solutions as transcendental equations:

$$k_1 = k_2 \tan(k_2 a), \tag{7}$$

$$k_1 = -k_2 \cot(k_2 a). \tag{8}$$

From these equations only a limited number of solutions exists for discrete values of E. The number and position of these solutions depend on a and V_0.

Now we look for solutions for unbound states, so $E > 0$. The incident particle, going in the positive x direction, can be reflected and transmitted at a change of boundary. Only in region 3 no particles are going in the negative x direction. For each of the three regions, the general solutions are therefore

$$\psi_1(x) = A_1 e^{ik_1 x} + B_1 e^{-ik_1 x}, \tag{9}$$

$$\psi_2(x) = A_2 e^{ik_2 x} + B_2 e^{-ik_2 x}, \tag{10}$$

$$\psi_3(x) = A_3 e^{ik_3 x}, \tag{11}$$

with $k_{1,3} = \sqrt{2mE/\hbar^2}$ and $k_2 = \sqrt{2m(E+V_0)/\hbar^2}$. The constants A_i and B_i are different from those of the bound states. Note that all exponentials represent travelling waves which can exist for any value of k (and therefore $E > 0$). We can set A_1 of the incoming wave arbitrarily to unity, which gives again four unknowns, together with the four equations of continuity of $\psi(x)$ and $\mathrm{d}\psi/\mathrm{d}x(x)$ at the two boundaries. The unbound solutions do not result in discrete values of E. Since the boundaries can transmit and reflect the incoming wave, we can define reflection R and transmission coefficients T as the ratio of the particle current densities j for reflected and transmitted waves.

From the amplitudes of $\psi(x)$ we get for the total transmission of the wave from region 1 to region 3, and the total reflection in region 1

$$R = \frac{\|B_1\|^2}{\|A_1\|^2}, \tag{12}$$

$$T = \frac{\|A_3\|^2}{\|A_1\|^2}, \tag{13}$$

using the solution and after some rearrangements gives

$$R = \frac{\frac{V_0^2}{4E(E+V_0)}\sin^2(a\sqrt{(\frac{2m}{\hbar^2}(E+V_0))})}{1+\frac{V_0^2}{4E(E+V_0)}\sin^2(a\sqrt{(\frac{2m}{\hbar^2}(E+V_0))})}, \tag{14}$$

$$T = \frac{1}{1+\frac{V_0^2}{4E(E+V_0)}\sin^2(a\sqrt{(\frac{2m}{\hbar^2}(E+V_0))})}. \tag{15}$$

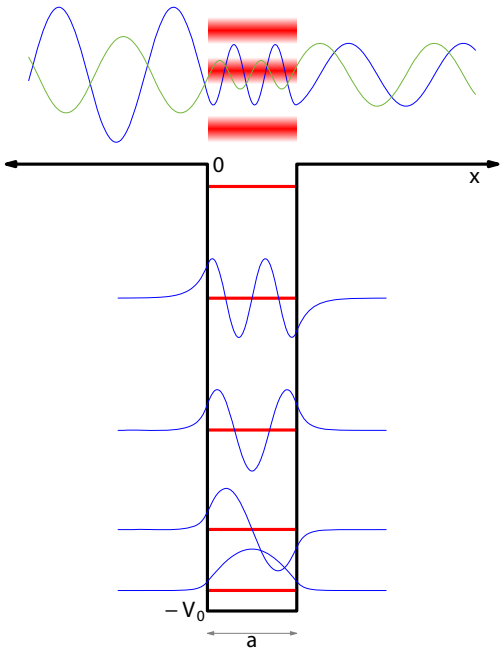

Fig. 3. Bound and unbound eigenstates of a one-dimensional quantum well. For $E < 0$ the solution of the Schrödinger equation gives several eigenstates, shown as red lines, together with the corresponding eigenfunctions which are real. The number of possible eigenstates depend on the potential depth V_0 and the well width a. All wave functions oscillate around zero, but are shown here with an offset of the energy eigenvalue. For $E > 0$, a solution corresponds to a plain wave of any energy. The plain wave, travelling from left to right, and for which the real and imaginary parts are shown, is partially transmitted and partially reflected at the potential well, depending on the energy. The total wave on the left interferes with the reflected wave, the transmitted wave has a constant absolute value of $|\psi|^2$. The interaction with the potential is illustrated as energy states with a very large width. In a real nuclear potential these quasi-bound states correspond to resonances with a definite spin and parity.

The sum of the transmission and reflection equals $R + T = 1$. This results from the assumption that the potential V is real. It is possible to include absorption by adding an imaginary part to the potential. For values of $E > 0$ where $\sin^2(k_2 a)$ equals zero, *i.e.* when

$$k_2 = \frac{n\pi}{a}\,, \tag{16}$$

with n an integer number, the transmission has its maximum value $T = 1$, and the reflection its minimum $R = 0$. These values are called resonances. So even if there are no discrete eigenvalues E as for the bound states, the energies corresponding to the resonances in the transmission are considered as unbound or quasi-bound states.

This situation is shown in fig. 3 with the one-dimensional quantum well together with the bound states represented by discrete line, and the quasi-bound states as diffuse bands.

In a three-dimensional situation we can also define an analogue quantum well around $r = 0$ and an incident particle arriving from $r = \infty$. The incident plane wave can be considered as an infinite sum of radial waves, the partial wave expansion. The outgoing wave is always a radial wave. In this case there is no transmission, only reflection and absorption. The principle remains the same and resonances occur also at quasi-bound states and these states even have a well defined spin and parity.

2.2 Introduction to the R-matrix formalism

If the wave functions of the nuclear system before and after the reaction were known, one could calculate the cross section with the usual concepts of reaction theory. While the incoming waves are known, the reaction modifies the outgoing wave functions in a generally unknown way.

The idea behind the R-matrix formalism is to use the wave function of the nuclear system of two particles when they are so close that they form a compound nucleus. Although the wave function of the compound nucleus is extremely complicated, one can expand it in its eigenstates. Matching then the incoming and outgoing waves to the internal wave function provides a way to describe the cross section of the reaction in terms of the properties of the eigenstates of the compound nucleus. These properties are basically the energy, spin, parity, and a set of partial widths related to the widths of the decay modes of the compound nucleus.

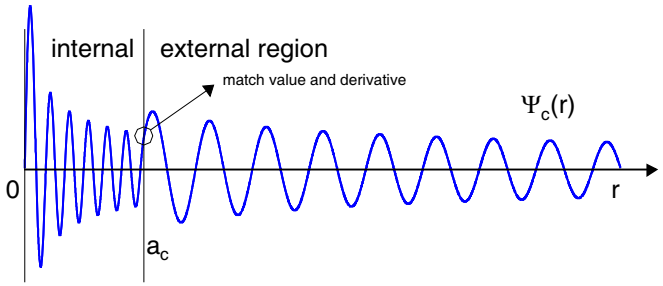

Fig. 4. Schematic view of the wave function of a channel as a function of the separation distance r. The wave function in the internal region $r < a_c$ is an expansion of the eigenstates of the compound nucleus. The full internal ($r < a_c$) wave function is not needed, only the value and derivative at $r = a_c$ where it matches the known external ($r > a_c$) wave function which is related to the Bessel functions.

This method of describing a reaction cross section using only the properties of nuclear excitation levels, is at the same time also the most important limitation. No information of the forces inside the nucleus is needed or can be extracted. The nucleus is treated as a black box of which the properties of the eigenstates have to be measured in order to describe the cross sections.

The binary nuclear reactions proceeding from one system of two particles to another system of two particles can be described with the general R-matrix theory. For neutron induced reactions, but also in other cases, such a reaction goes often through the formation of a compound nucleus X^*:

$$A + a \rightarrow X^* \rightarrow B + b. \tag{17}$$

The R-matrix formalism does not only apply to compound nucleus reactions. Both direct and indirect reactions can be described with it. The inclusion of the Coulomb interaction allows us to use it also for charged particle reactions. But the theory is applicable only in a general way for binary reactions which is appropriate for neutron induced reactions up to energies of several tens of MeV.

In a very general way, the cross section of a two-body nuclear reaction could be calculated if the nuclear wave functions were known. The wave functions could be calculated by solving the Schrödinger equation for the nuclear system. This requires that the nuclear potential is known. When the two particles are far away, the interaction can be considered absent for neutral particles or to be the Coulomb interaction for charged particles. In these cases it is indeed possible to calculate the wave functions.

When the two particles are so close to each other that a nuclear reaction takes place, the potential of the interaction is extremely complicated. For certain energy ranges and reactions this potential can still be approximated or calculated [29] and the wave functions and cross sections can be calculated. In other cases however, and especially in the resolved resonance region, the complexity of the reacting system does not allow this.

The first step is to consider that the reaction process can be split up geometrically into two regions for each channel where a channel is the precise constellation of particles and their spins. If the separation is smaller than the channel radius a_c, all nucleons involved in the reaction are close to each other and form a compound nucleus. Although the wave function of the compound nucleus is extremely complicated, it can be expanded as a linear combination of its eigenstates without solving explicitly the Schrödinger equation of the system. In the external region, at distances larger than a_c, the potential is zero for neutral particles or is the Coulomb interaction for charged particles and the Schrödinger equation of the system can be solved. The properties of the eigenstates of the compound nucleus are included in the R-matrix. Equating the values and derivatives of the wave functions at the boundary of the internal and external region assures a smooth wave function and the cross sections can be calculated. The exact internal wave function is not needed, only the values and derivatives at the nuclear surface, as illustrated in fig. 4.

In the following we describe in more detail the R-matrix formalism which links the properties of the nuclear states to the cross sections. The cross section in the thermal energy region is also described by the R-matrix formalism. Reaction cross sections at thermal energy are the sum of the contributions of all nuclear states, *i.e.* the resonances but also the bound states, sometimes referred to as "negative energy" resonances. Other reaction formalisms have been used in the past, like the K-matrix formalism [30] still in use for particle physics [31], but for neutron-induced resonance reactions the R-matrix formalism, and in particular one of its approximations, is nowadays the preferred formalism.

The R-matrix formalism was first introduced by Wigner and Eisenbud [32]. A most extensive and detailed overview has been given by Lane and Thomas [24] and by Lynn [33]. Recently Fröhner [34] summarized the R-matrix formalism with a focus on neutron-induced reactions together with other useful considerations on nuclear data evaluation. An excellent review of the theory was more recently given by Descouvemont and Baye [35]. Other related references of interest can be found elsewhere [36–45]. A brief outline of the formalism will be given in order to understand its basic principles.

2.2.1 Channel representation

It is customary to use the concept of channels in the description of nuclear reactions, which will be limited to two particle reactions in the following. The entrance channel c consists of a particular initial constellation of particles and all the quantum numbers necessary to describe the corresponding partial wave function. The type of the two particles α_1 and α_2, with their spins I_{α_1} and I_{α_2}, and their states of internal excitation, are denoted by α. Four quantum numbers are needed to include the spins of the particles in a channel. The most appropriate combination is the orbital angular momentum ℓ, the channel spin s, which is the combined spin of the two particles,

$$\boldsymbol{s} = \boldsymbol{I}_{\alpha_1} + \boldsymbol{I}_{\alpha_2}, \tag{18}$$

the total angular momentum J,

$$\boldsymbol{J} = \boldsymbol{s} + \boldsymbol{\ell}, \tag{19}$$

and its projection on the z-axis m_J. So the entrance channel c can be designated by

$$c = \{\alpha, \ell, s, J, m_J\}. \tag{20}$$

Similarly, the exit channel is given by

$$c' = \{\alpha', \ell', s', J', m'_J\}. \tag{21}$$

The reaction $\alpha \rightarrow \alpha'$ may go through the formation of a compound nucleus, like often the case with neutron-induced reactions. The reaction can then be written as $\alpha \rightarrow A^* \rightarrow \alpha'$. The spin and parity are of course conserved in all stages of the reaction and the compound nucleus has its defined spin J and parity π. The conservation of spin and parity puts restrictions on the entrance channels that are open to form the compound nucleus or the exit channels open for the decay of the compound nucleus. For neutrons and protons the intrinsic spin is 1/2 and the intrinsic parity is positive. Conservation of angular momentum gives the vector addition:

$$\boldsymbol{J} = \boldsymbol{I}_{\alpha_1} + \boldsymbol{I}_{\alpha_2} + \boldsymbol{\ell} = \boldsymbol{I}_{\alpha'_1} + \boldsymbol{I}_{\alpha'_2} + \boldsymbol{\ell}' \tag{22}$$

and conservation of parity gives, using $+1$ for positive and -1 for negative parity,

$$\pi = \pi_{I_{\alpha_1}} \times \pi_{I_{\alpha_2}} \times (-1)^{\ell} = \pi_{I_{\alpha'_1}} \times \pi_{I_{\alpha'_2}} \times (-1)^{\ell'}. \tag{23}$$

The conservation of angular momentum has important consequences for cross section calculations based on channels. The total number of possible combinations to sum the spins and orbital momentum is $(2I_{\alpha_1}+1)(2I_{\alpha_2}+1)(2\ell+1)$. Only $2J+1$ orientations of them add up to J. For this reason in expressions for cross sections of the formation of a compound nucleus level with spin J for a given ℓ the statistical factor $g(J)$,

$$g(J) = \frac{2J+1}{(2I_{\alpha_1}+1)(2I_{\alpha_2}+1)}, \tag{24}$$

has to be taken into account.

For a neutron having spin $i = 1/2$, incident on a nucleus with spin, several combinations are possible to arrive at a final spin J. From the combinations given in table 1, it can be seen that a state with the same spin and parity can be reached by different partial waves.

The boundary $r = a_c$ is the limit between the internal region, where all the nucleons interact, and the external region where the incident and target particles do not have a nuclear interaction, other than possibly a Coulomb interaction. Although there is no sharp limit, in practice the channel radius a_c can be taken just slightly larger than the radius $R' = R_0 A^{1/3}$ of a spherical nuclear volume with $A = A_{\alpha_1} + A_{\alpha_2}$ nucleons, and where for R_0 usually the value 1.35 fm is used. This scattering radius can be used as a first approximation of the low-energy potential scattering cross section σ_{pot} with the relation

$$\sigma_{\mathrm{pot}} = 4\pi R'^2. \tag{25}$$

Experimental values of R' show larger structures around the smooth curve $R' = R_0 A^{1/3}$ which can be well described with optical model calculations. In evaluated nuclear libraries the channel radius a_c can be defined to have either the numerical value of a possibly energy-dependent scattering radius R', or an energy-independent, mass-dependent channel radius given by

$$a_c = 0.8 + 1.23 A'^{1/3}\,\mathrm{fm}, \tag{26}$$

where A' is the ratio of the isotope mass to the mass of the neutron. The channel is defined in the center of mass and the reduced mass of the particles is

$$m_c = m_\alpha = \frac{m_{\alpha_1} m_{\alpha_2}}{m_{\alpha_1} + m_{\alpha_2}} \tag{27}$$

Table 1. The spin combinations for an incident neutron (with spin $i = 1/2$) on a target nucleus with spin $I = 0$, $I = 1/2$, and $I = 1$, with relative orbital momentum $\ell = 0$ (s-wave), $\ell = 1$ (p-wave), and $\ell = 2$ (d-wave). For completeness, the spin statistical factors $g_s = (2s+1)/((2i+1)(2I+1))$ and $g_J = (2J+1)/((2s+1)(2\ell+1))$ are also given. Only the case for a positive parity nucleus is shown, for negative parity all signs must be inverted.

I	ℓ	J	s	g_s	g_J
0^+	0	$1/2^+$	1/2	1	1
0^+	1	$1/2^-$	1/2	1/3	1
0^+	1	$3/2^-$	1/2	2/3	2
0^+	2	$3/2^+$	1/2	2/5	2
0^+	2	$5/2^+$	1/2	3/5	3
$1/2^+$	0	0^+	0	1	1/4
$1/2^+$	0	1^+	1	1	3/4
$1/2^+$	1	1^-	0	1	3/4
$1/2^+$	1	0^-	1	1/9	1/4
$1/2^+$	1	1^-	1	1/3	3/4
$1/2^+$	1	2^-	1	5/9	5/4
$1/2^+$	2	2^+	0	1	5/4
$1/2^+$	2	1^+	1	1/5	3/4
$1/2^+$	2	2^+	1	1/3	5/4
$1/2^+$	2	3^+	1	7/15	7/4
1^+	0	$1/2^+$	1/2	1	1/3
1^+	0	$3/2^+$	3/2	1	2/3
1^+	1	$1/2^-$	1/2	1/3	1/3
1^+	1	$3/2^-$	1/2	2/3	2/3
1^+	1	$1/2^-$	3/2	1/6	1/3
1^+	1	$3/2^-$	3/2	1/3	2/3
1^+	1	$5/2^-$	3/2	1/2	1
1^+	2	$3/2^+$	1/2	2/5	2/3
1^+	2	$5/2^+$	1/2	3/5	1
1^+	2	$1/2^+$	3/2	1/10	1/3
1^+	2	$3/2^+$	3/2	1/5	2/3
1^+	2	$5/2^+$	3/2	3/10	1
1^+	2	$7/2^+$	3/2	2/5	4/3

the wave number k, related to the de Broglie wavelength $\lambda\!\!\!^{-}$, is

$$k_c = k_\alpha = \frac{1}{\lambda\!\!\!^{-}_c} = \sqrt{\frac{2m_\alpha E_\alpha}{\hbar^2}} \tag{28}$$

and the relative velocity is

$$v_c = v_\alpha = \hbar k_c / m_c. \tag{29}$$

The dimensionless distance ρ_c is used to indicate the distance r_c in measures of de Broglie wavelengths,

$$\rho_c = \rho_\alpha = k_c r_c. \tag{30}$$

2.2.2 The wave function in the external region

The system of the two particles interacting through a central potential $V(r)$ can be described by the Schrödinger equation of the motion of the reduced mass particle. Also, using spherical coordinates, the solution $\psi(r, \theta, \phi)$ can, in case of a central potential, be separated in a radial and an angular part

$$\psi(r, \theta, \phi) = R(r)\Theta(\theta)\Phi(\phi). \tag{31}$$

The radial part $R(r)$ still depends on the non-negative integer solutions $\ell(\ell+1)$ of $\Theta(\theta)$. The integers appearing in the solution of $\Phi(\phi)$ are $m_\ell = 0, \pm 1, \pm 2 \ldots \pm \ell$. The solutions of the angular part $\Theta(\theta)\Phi(\phi)$ do not depend on the

Table 2. The spherical Bessel functions and the incoming and outgoing waves from eqs. (35) and (36). Derived quantities are given in table 3.

ℓ	j_ℓ	n_ℓ	$O_\ell = I_\ell^*$
0	$\frac{\sin\rho}{\rho}$	$-\frac{\cos\rho}{\rho}$	$e^{i\rho}$
1	$\frac{\sin\rho}{\rho^2} - \frac{\cos\rho}{\rho}$	$-\frac{\cos\rho}{\rho^2} - \frac{\sin\rho}{\rho}$	$e^{i\rho}\left(\frac{1}{\rho} - i\right)$
ℓ	$(-1)^\ell \rho^\ell \left(\frac{1}{\rho}\frac{\mathrm{d}}{\mathrm{d}\rho}\right)^\ell \frac{\sin\rho}{\rho}$	$-(-1)^\ell \rho^\ell \left(\frac{1}{\rho}\frac{\mathrm{d}}{\mathrm{d}\rho}\right)^\ell \frac{\cos\rho}{\rho}$	

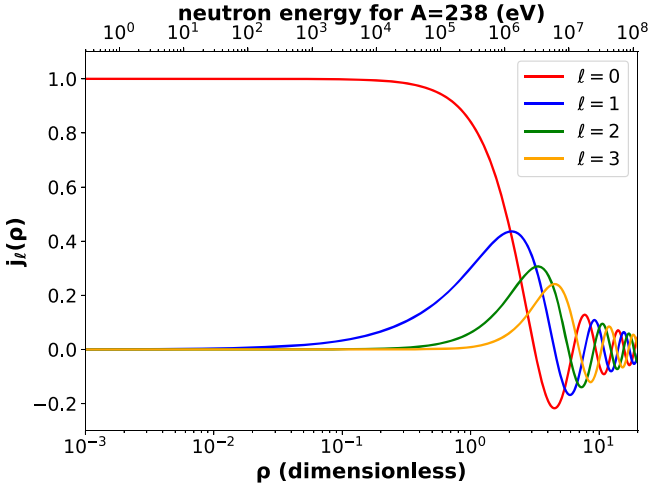

Fig. 5. The spherical Bessel functions $j_\ell(\rho)$ for $\ell = 0, 1, 2, 3$ are shown as a function of the dimensionless variable $\rho = kr$ and as a function of equivalent energy for a nucleus with mass $A = 238$.

central potential and are the spherical harmonics $Y_{m_\ell}^\ell(\theta, \phi)$. Only the solution $R(r)$ of the radial part depends on the potential $V(r)$. The equation for the radial part,

$$\left[\frac{1}{r^2}\frac{\mathrm{d}}{\mathrm{d}r}\left(r^2\frac{\mathrm{d}}{\mathrm{d}r}\right) - \frac{\ell(\ell+1)}{r^2} - \frac{2m_c}{\hbar^2}\big(V(r) - E\big)\right] R(r) = 0, \tag{32}$$

can be simplified by introducing

$$u(r) = rR(r), \tag{33}$$

giving rise to what we will call now the radial Schrödinger equation, and which shows much similarity to the equation for the one-dimensional case:

$$\left[\frac{\mathrm{d}^2}{\mathrm{d}r^2} - \frac{\ell(\ell+1)}{r^2} - \frac{2m_c}{\hbar^2}\big(V(r) - E\big)\right] u(r) = 0. \tag{34}$$

This equation can be solved for the case of the Coulomb potential $V(r) = -Z_{\alpha_1} Z_{\alpha_2} e^2/(4\pi\epsilon_0 r)$. The general solution is a linear combination of regular and irregular Coulomb wave functions. In the special case that $V(r) = 0$, such as for neutrons, eq. (34), after a rearrangement in dimensionless form, is called the spherical Bessel equation. The solution consists of a linear combination of spherical Bessel functions of the first type $j_\ell(\rho)$, and of the second type $n_\ell(\rho)$ (or Neumann functions). Two linearly independent complex combinations of j_ℓ and n_ℓ are known as spherical Bessel functions of the third type (or Hankel functions) $h_\ell^+(\rho)$ and $h_\ell^-(\rho)$ [46,47]. These are functions of the dimensionless parameter $\rho = kr$. Although $n_\ell(\rho) \to -\infty$ for $r \to 0$, this irregular solution should be included because we only need this solution in the external region $r > a_c$. The appropriate solution for a channel c is a linear combination of waves corresponding to incoming $I_c(r)$ and outgoing $O_c(r)$ waves for a free particle, $R(r) = R_\ell(r) = y_\ell I_\ell(r) + x_\ell O_\ell(r)$, with

$$I_c(r) = I_\ell(r) = -i\rho h_\ell^-(\rho) = -i\rho(j_\ell(\rho) - in_\ell(\rho)) \tag{35}$$

and

$$O_c(r) = O_\ell(r) = -i\rho h_\ell^+(\rho) = i\rho(j_\ell(\rho) + in_\ell(\rho)). \tag{36}$$

At large separation distances $r \to \infty$ the asymptotic forms of $I(r)$ and $O(r)$ correspond indeed to plain waves travelling in positive direction (outgoing waves) or negative direction (incoming waves). The functions $j_\ell(\rho)$ and $n_\ell(\rho)$ together with $O_\ell(\rho)$ are given in table 2. In fig. 5 the function $j_\ell(\rho)$ is shown as a function of ρ and as a function of equivalent energy for a nucleus with mass $A = 238$.

2.2.3 The collision matrix $\boldsymbol{U}$

The total wave function Ψ in the external region can be expressed as the superposition of all incoming and outgoing partial waves $\mathcal{I}_c$ and $\mathcal{O}_c$, with amplitudes y_c and x_c, and summed over all possible channels c,

$$\Psi = \sum_c y_c \mathcal{I}_c + \sum_{c'} x_{c'} \mathcal{O}'_c. \tag{37}$$

The complete wave functions in the channel, $\mathcal{I}_c$ and $\mathcal{O}_c$, contain the radial parts I_c and O_c, but also the angular part of relative motion $Y^\ell_{m_\ell}$, as well as the internal wave functions of the particles and the channel spin, combined in φ_c, and are written as

$$\mathcal{I}_c = I_c r^{-1} \varphi_c i^\ell Y^\ell_{m_\ell}(\theta, \phi)/\sqrt{v_c} \tag{38}$$

and

$$\mathcal{O}_c = O_c r^{-1} \varphi_c i^\ell Y^\ell_{m_\ell}(\theta, \phi)/\sqrt{v_c}. \tag{39}$$

The factor $1/\sqrt{v_c}$ normalizes the waves to unit flux. The physical process of the reaction will result in a modification of the outgoing waves. In the reaction the coefficients x_c of the outgoing waves, depending on the details of the reaction which are observable in the cross section, have to be determined with respect to the coefficients of the incoming waves y_c. The collision matrix $U_{cc'}$ is now defined as the relation between the coefficients of the incoming and outgoing waves:

$$x_{c'} \equiv -\sum_c U_{c'c} y_c. \tag{40}$$

All the physics of the reaction is contained in the elements of the collision matrix. The collision matrix has two important properties. From the conservation of probability flux in the reaction it follows that the collision matrix is unitary, which means that its complex conjugate equals its reciprocal, $\mathbf{U}^* = \mathbf{U}^{-1}$, or

$$\sum_c U^*_{cc'} U_{cc''} = \delta_{c'c''}. \tag{41}$$

The second property follows from time reversal conservation and implies that the collision matrix is symmetric, $U_{cc'} = U_{c'c}$.

Finally we can express the total wave function of eq. (37) in terms of the collision matrix:

$$\Psi = \sum_c y_c \left(\mathcal{I}_c - \sum_{c'} U_{cc'} \mathcal{O}_{c'} \right), \tag{42}$$

which is a linear combination of the wave functions for each channel c, consisting of an ingoing wave and the modified outgoing waves summed over all channels c'.

2.2.4 The relation between the cross sections and the collision matrix $\mathbf{U}$

The relation between reaction cross section and wave functions, describing a probability, is based on the conservation of probability density. The probability density of an incident plain wave, which is the flux of particles $\boldsymbol{j}_\varphi$ is given by the quantum mechanical expression

$$\boldsymbol{j}_\varphi = \frac{\hbar}{2mi} \left(\psi^* \nabla \psi - \psi \nabla \psi^* \right). \tag{43}$$

The connection with the cross section is best illustrated by considering a flux of incident particles j_{inc}, represented by a plain wave ψ_{inc} which can be expanded in a series of partial radial waves, scattering elastically at a point $r = 0$ because of an unknown physical process. The scattered wave, originating at $r = 0$ is a radial wave ψ_{sc} and far from the scattering center at a distance r in a solid angle element $\mathrm{d}\Omega$ the current of scattered particles across the surface $r^2 \mathrm{d}\Omega$ is j_{sc}. The total wave $\psi = \psi_{\text{inc}} + \psi_{\text{sc}}$ is a solution of the Schrödinger equation for this system. The cross section of this reaction, which is a differential cross section, is defined as

$$\mathrm{d}\sigma = \frac{j_{\text{sc}}}{j_{\text{inc}}} r^2 \mathrm{d}\Omega. \tag{44}$$

Integrating over $\mathrm{d}\Omega$ gives the total scattering cross section. If elastic scattering were the only process to occur, the total current of ingoing particles equals that of the outgoing particles. Any reaction, defined as any other process than elastic scattering, means that there is a difference in the absolute values of the ingoing and outgoing current.

In the more general description of channels the total wave function is eq. (42). Elastic scattering means here that the entrance and exit channel are the same. A change of channel in the outgoing wave is considered as a reaction. With a similar approach, including the expansion of the incoming plane wave into an infinite sum of partial waves ℓ, and using the full description of the channel wave functions, the angular differential cross section for the reaction $\alpha \to \alpha'$ has been worked out by Blatt and Biedenharn [48]. For zero Coulomb interaction the expression using the partial wave expansion is in a very general way

$$\frac{\mathrm{d}\sigma_{\alpha\alpha'}}{\mathrm{d}\Omega} = \lambda\!\!\!^{-2} \sum_{L=0}^{\infty} B_{L\alpha\alpha'} P_L(\cos\theta), \tag{45}$$

where P_L is the Legendre polynomial of degree L (and is unrelated to the penetrability factor P_ℓ of eq. (66)). The coefficients $B_{L\alpha\alpha'}$ are rather complicated factors and contain summing over the collision matrix elements $U_{cc'}$ and relations containing Clebsch-Gordan coefficients for the spin bookkeeping. These are non-zero only if $|\ell - \ell'| < L < \ell + \ell'$ and $\ell + \ell' - L$ is even, *i.e.* $(-1)^{\ell+\ell'} = (-1)^L$. The cross section for an interaction from channel c to channel c' is

$$\sigma_{cc'} = \pi \lambda\!\!\!^{-2}_c |\delta_{c'c} - U_{c'c}|^2. \tag{46}$$

If the interaction occurs without a change in the channel c then the process is called elastic scattering. The cross section is, putting $c' = c$,

$$\sigma_{cc} = \pi \lambda\!\!\!^{-2}_c |1 - U_{cc}|^2 \tag{47}$$

and the cross section for a channel reaction, *i.e.* any interaction which is not elastic scattering, is obtained by summing (46) over all c', except c,

$$\sigma_{cr} = \pi \lambda\!\!\!^{-2}_c (1 - |U_{cc}|^2) \tag{48}$$

and the total cross section is obtained by summing all channels c'

$$\sigma_{c,T} = \sigma_c = 2\pi \lambda\!\!\!^{-2}_c (1 - \mathrm{Re}\, U_{cc}). \tag{49}$$

In practice, channel-to-channel cross sections are often not directly observable. One would like to have the cross sections $\alpha \to \alpha'$ for the component of total angular momentum J for reactions leading from the entrance pair of particles in a particular state α to the exit pair α' which requires summing over the appropriate channels. The total reaction cross section is obtained by integrating (45) over the full solid angle to obtain the total cross section for the component of total angular momentum J,

$$\sigma_{\alpha\alpha'}(J) = \pi \lambda\!\!\!^{-2}_\alpha g(J) \sum_{s,s',\ell,\ell'} |\delta_{ss'\ell\ell'} - U_{s\ell,s'\ell'}|^2, \tag{50}$$

and the total cross section by summing over all α'

$$\sigma_{\alpha,T}(J) = 2\pi \lambda\!\!\!^{-2}_\alpha g(J) \sum_{s,\ell} (1 - \mathrm{Re}\, U_{s\ell,s\ell}). \tag{51}$$

2.2.5 The wave function in the internal region

The complete wave function Ψ can be described as the product of the function of relative motion and the channel-spin function, giving the internal states of the particles α_1 and α_2 and their combined spin. From the function of relative motion the radial wave function $u(r)$ is separated and the remaining part is combined with the channel-spin function to give the channel surface function φ_c so that at the boundary $r = a_c$

$$\Psi = \sum_c \varphi_c u_c(a_c). \tag{52}$$

The surface functions φ_c have the property of orthonormality over the surface S_c given by $r = a_c$. This will be exploited to expand certain quantities in terms of surface functions. From eq. (52) follows immediately that

$$u_c(a_c) = \int \varphi_c^* \Psi \mathrm{d}S_c. \tag{53}$$

The integration over a surface, instead of integrating over a volume, is particularly useful in deriving the R-matrix relation using Green's theorem, expressing a volume integral in a surface integral.

At the channel surface $r = a_c$ the radial wave function for the internal and external region should match. For the internal wave function at $r = a_c$, the value V_c and derivative D_c are defined with a normalization constant as

$$\begin{aligned} V_c &= \sqrt{\frac{\hbar^2}{2m_c a_c}} u_c(a_c), \\ &= \sqrt{\frac{\hbar^2}{2m_c a_c}} \int \varphi_c^* \Psi \, \mathrm{d}S_c \end{aligned} \tag{54}$$

and

$$\begin{aligned} D_c &= \sqrt{\frac{\hbar^2}{2m_c a_c}} a_c \left(\frac{\mathrm{d}u_c}{\mathrm{d}r} \right)_{r=a_c}, \\ &= \sqrt{\frac{\hbar^2}{2m_c a_c}} \int \varphi_c^* \nabla_n (r\Psi) \mathrm{d}S_c, \\ &= V_c + \sqrt{\frac{\hbar^2}{2m_c a_c}} a_c \int \varphi_c^* \mathrm{d}S_c. \end{aligned} \tag{55}$$

In the internal region the wave function cannot be calculated readily by solving the Schrödinger equation since the nuclear potential is in general very complicated and the nucleus has many interacting nucleons. But the wave function can be expressed as an expansion in eigenfunctions X_λ at energies E_λ

$$\Psi = \sum_\lambda A_\lambda X_\lambda \tag{56}$$

and the coefficients A_λ can be expressed as

$$A_\lambda = \int X_\lambda^* \Psi \, \mathrm{d}\tau, \tag{57}$$

where the integration goes over the volume $\mathrm{d}\tau$ of the internal region given by $r < a_c$.

The values and derivatives on the surface $r = a_c$ are defined, analogically to eq. (54) and (55), as

$$\gamma_{\lambda c} = \sqrt{\frac{\hbar^2}{2m_c a_c}} \int \varphi_c^* X_\lambda \, \mathrm{d}S_c \tag{58}$$

and

$$\delta_{\lambda c} = \gamma_{\lambda c} + \sqrt{\frac{\hbar^2}{2m_c a_c}} a_c \int \varphi_c^* \nabla_n (X_\lambda) \mathrm{d}S_c. \tag{59}$$

The boundary conditions to be satisfied on the channel surface are taken identical for all λ

$$B_c = \delta_{\lambda c} / \gamma_{\lambda c}. \tag{60}$$

Applying Green's theorem to eq. (57) gives

$$\begin{aligned} A_\lambda &= \int X_\lambda^* \Psi \, \mathrm{d}\tau \\ &= (E_\lambda - E)^{-1} \frac{\hbar^2}{2m_c} \int (X_\lambda^* \nabla_n(\Psi) - \Psi \nabla_n(X_\lambda^*)) \, \mathrm{d}S_c \\ &= (E_\lambda - E)^{-1} \sum_c (D_c - B_c V_c) \gamma_{\lambda c}, \end{aligned} \tag{61}$$

using eqs. (54), (55), (58), (59) and (60). The expression (56) for the wave function can now be written as

$$\Psi = \sum_c \left[\sum_\lambda \frac{X_\lambda \gamma_{\lambda c}}{E_\lambda - E} \right] (D_c - B_c V_c). \tag{62}$$

Table 3. The penetrability P_ℓ, the level shift S_ℓ and the hard-sphere phase shift ϕ_ℓ for reaction channels without Coulomb interaction, as a function of $\rho = ka_c$. These parameters are derived from the quantities in table 2.

ℓ	P_ℓ	S_ℓ	ϕ_ℓ
0	ρ	0	ρ
1	$\rho^3/(1+\rho^2)$	$-1/(1+\rho^2)$	$\rho - \arctan\rho$
ℓ	$\frac{\rho^2 P_{\ell-1}}{(\ell-S_{\ell-1})^2+P_{\ell-1}^2}$	$\frac{\rho^2(\ell-S_{\ell-1})}{(\ell-S_{\ell-1})^2+P_{\ell-1}^2} - \ell$	$\phi_{\ell-1} - \arctan\frac{P_{\ell-1}}{\ell-S_{\ell-1}}$

By multiplying each side of eq. (62) by $\varphi_{c'}$, integrating over the surface $r = a_c$ and using eq. (58) one obtains

$$V_{c'} = \sum_c R_{cc'}(D_c - B_c V_c), \tag{63}$$

with

$$R_{cc'} = \sum_\lambda \frac{\gamma_{\lambda c}\gamma_{\lambda c'}}{E_\lambda - E}\,. \tag{64}$$

The quantity $R_{cc'}$ is the R-matrix and contains the properties E_λ and $\gamma_{\lambda c}$ of the eigenstates λ. The boundary constant B_c can be chosen freely.

2.2.6 The relation between the R-matrix and the collision matrix $\mathbf{U}$

The values and derivatives of the internal wave function are given by the R-matrix relation eq. (63). The external wave function is given by eq. (42) and is known except for the boundary conditions. The boundary condition is that both the internal and external wave functions have the same value and radial derivative at $r = a_c$ in order to have a smooth transition. By matching these conditions and after considerable rearrangements, the collision matrix $U_{cc'}$ can be given explicitly as a function of the R-matrix $R_{cc'}$ in matrix notation by

$$\mathbf{U} = \boldsymbol{\Omega}\mathbf{P}^{1/2}[\mathbf{1} - \mathbf{R}(\mathbf{L} - \mathbf{B})]^{-1}[\mathbf{1} - \mathbf{R}(\mathbf{L}^* - \mathbf{B})]\mathbf{P}^{-1/2}\boldsymbol{\Omega}. \tag{65}$$

The matrices $\boldsymbol{\Omega}$, $\mathbf{P}$, $\mathbf{1}$, $\mathbf{L}$ and $\mathbf{B}$ in eq. (65) are square diagonal matrices. Only the symmetric and unitary matrices $\mathbf{U}$ and $\mathbf{R}$ can have non-zero off-diagonal elements. The introduced complex matrix $\mathbf{L}$ is given by

$$L_c = \left(\frac{\rho}{O_c}\frac{\mathrm{d}O_c}{\mathrm{d}\rho}\right)_{r=a_c} = S_c + iP_c, \tag{66}$$

where the real matrix S_c is called the shift factor and P_c the penetrability factor. The matrix Ω_c is defined by

$$\Omega_c = \left(\frac{I_c}{O_c}\right)_{r=a_c}, \tag{67}$$

which can be reduced for neutral particles, using eqs. (35) and (36), to

$$\Omega_c = \exp(-i\phi_c), \tag{68}$$

from which ϕ_c follows:

$$\phi_c = \arg O_c(a_c) = \arctan\left(\frac{\mathrm{Im}\,O_c}{\mathrm{Re}\,O_c}\right) = \arctan\left(-\frac{j_\ell(\rho)}{n_\ell(\rho)}\right). \tag{69}$$

A list of P_ℓ, S_ℓ and ϕ_ℓ is given in table 3. They are directly related to the solution of the Schrödinger equation in the external region, which are the spherical Bessel and Neumann functions $j_\ell(\rho)$ and $n_\ell(\rho)$ for neutral particles, and can be derived from the quantities listed in table 2.

If the boundary conditions B_c, defined by eq. (60), are real, then the $\delta_{\lambda c}$ and the $\gamma_{\lambda c}$ are real and hence $\mathbf{R}$ is real. In addition $\mathbf{R}$ is symmetrical. A common choice is to take

$$B_c = S_c, \tag{70}$$

which eliminates the shift factor for s-waves, but introduces an energy dependence. The choice $B_c = -\ell$ has also been proposed [34]. At low energy this is equivalent as can be seen in fig. 6, where P_ℓ, S_ℓ and ϕ_ℓ are plotted as a function of ρ and as a function of equivalent energy for a nucleus with mass $A = 238$.

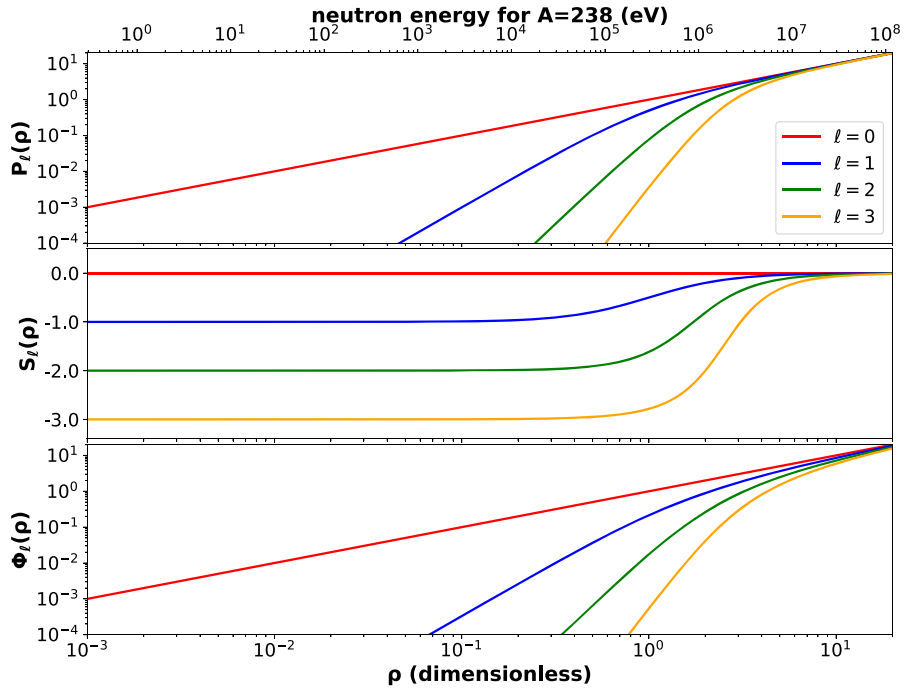

Fig. 6. The functions $P_\ell(\rho)$, $S_\ell(\rho)$ and $\phi_\ell(\rho)$ for $\ell = 0, 1, 2, 3$ shown as a function of the dimensionless variable ρ and as a function of equivalent energy for a nucleus with mass $A = 238$.

So eq. (65) defines the collision matrix in terms of the parameters of the R-matrix, $\gamma_{\lambda c}$ and E_λ, representing the physical process of the reaction, and the quantities P_c, S_c, ϕ_c, describing the known incoming and outgoing waves I_c and O_c, outside a sphere with radius a_c. The values B_c determine the boundary conditions at the matching point of the internal and external region, and are free to be chosen. The unknowns of the R-matrix, $\gamma_{\lambda c}$ and E_λ, need to be determined in order to know the U-matrix and subsequently the cross sections.

2.3 Approximations of the R-matrix

Several approximations of the R-matrix have been developed in the past in order to overcome the complications of inverting the matrix

$$[\mathbf{1} - \mathbf{R}(\mathbf{L} - \mathbf{B})]^{-1},$$

appearing in eq. (65). Except in the case where only 1 or 2 channels are involved, the inversion is in general impossible without additional assumptions. The problem can be put in terms of the inversion of a level matrix $\mathbf{A}$ of which the elements refer to the properties of the levels λ of the system. The problem of inverting a matrix concerning all channels is now put in a problem of inverting a matrix concerning levels.

The level matrix $A_{\lambda\mu}$ is introduced by putting the following form:

$$\left([\mathbf{1} - \mathbf{R}(\mathbf{L} - \mathbf{B})]^{-1}\right)_{cc'} = \delta_{cc'} + \sum_{\lambda\mu} \gamma_{\lambda c}\gamma_{\mu c'}(L_{c'} - B_{c'})A_{\lambda\mu}, \tag{71}$$

from which the elements of the inverse of $\mathbf{A}$ are

$$\begin{aligned}\left(\mathbf{A}^{-1}\right)_{\lambda\mu} &= (E_\lambda - E)\delta_{\lambda\mu} - \sum_c \gamma_{\lambda c}\gamma_{\mu c}(L_c - B_c) \\ &= (E_\lambda - E)\delta_{\lambda\mu} - \Delta_{\lambda\mu} - \frac{1}{2}i\Gamma_{\lambda\mu},\end{aligned} \tag{72}$$

with the quantities $\Delta_{\lambda\mu}$ and $\Gamma_{\lambda\mu}$ defined by

$$\Delta_{\lambda\mu} = \sum_c (S_c - B_c)\gamma_{\lambda c}\gamma_{\mu c} \tag{73}$$

and

$$\Gamma_{\lambda\mu} = 2\sum_c P_c \gamma_{\lambda c}\gamma_{\mu c}. \tag{74}$$

Now the collision matrix from eq. (65) can be expressed in terms of **A**

$$U_{cc'} = \Omega_c \Omega_{c'} \left(\delta_{cc'} + 2i\sqrt{P_c P_{c'}} \sum_{\lambda\mu} A_{\lambda\mu}\gamma_{\lambda c}\gamma_{\mu c'} \right). \tag{75}$$

Additional approximations have been formulated in order to simplify this expression. The most illustrative is the Breit and Wigner Single Level (SLBW) approximation where only one level is considered. It can be extended to several, independent levels, which is the Breit and Wigner Multi Level (MLBW) approximation. The formalism of Reich and Moore [49] neglects only the off-diagonal contributions of the photon channels, which is an accurate approximation for medium and heavy nuclei. It takes into account the interference between levels and reduces to the BWSL approximation in the limit of a single level. These three formalisms will be described in some more detail. Other formalisms exist of which we mention here the formalisms of Kapur and Peierls [50], Wigner and Eisenbud [32], Adler and Adler [39], Hwang [51] and more recently Luk'yanov and Yaneva [44].

2.3.1 The Breit-Wigner single level approximation

The expression eq. (72) can be simplified if only a single level is present. In that case the matrix contains only a single element. Therefore

$$\left(\mathbf{A}^{-1}\right)_{\lambda\mu} = A^{-1} = E_\lambda - E + \Delta_\lambda - i\Gamma_\lambda/2, \tag{76}$$

with

$$\Delta_\lambda = \Delta_{\lambda\lambda} = -\sum_c (S_c - B_c)\gamma_{\lambda c}^2 \tag{77}$$

and

$$\Gamma_\lambda = \Gamma_{\lambda\lambda} = \sum_c \Gamma_{\lambda c} = \sum_c 2P_c\gamma_{\lambda c}^2. \tag{78}$$

Substituting these expressions in eq. (75) gives the collision matrix

$$U_{cc'} = e^{-i(\phi_c+\phi_{c'})}\left(\delta_{cc'} + \frac{i\sqrt{\Gamma_{\lambda c}\Gamma_{\mu c'}}}{E_\lambda + \Delta_\lambda - E - i\Gamma_\lambda/2}\right). \tag{79}$$

From the collision matrix the cross sections can be calculated. For the total cross section this results in

$$\sigma_c = \pi\lambda\!\!\!^{-2}_c g_c \left(4\sin^2\phi_c + \frac{\Gamma_\lambda\Gamma_{\lambda c}\cos 2\phi_c + 2(E - E_\lambda - \Delta_\lambda)\Gamma_{\lambda c}\sin 2\phi_c}{(E - E_\lambda - \Delta_\lambda)^2 + \Gamma_\lambda^2/4}\right). \tag{80}$$

The first part of the total cross section is the potential scattering or hard sphere scattering cross section $\sigma_p = 4\pi\lambda\!\!\!^{-2}_c g_c \sin^2\phi_c$. It is associated with the elastic scattering of the incoming neutron from the potential of the nucleus without forming a compound state. The term with the factor $\sin 2\phi_c$ is the interference of the potential scattering and the resonant elastic scattering through formation of a compound nucleus. Finally the term with $\cos 2\phi_c$ describes the resonance cross sections of the channels.

In a more practical case we can see what the cross sections becomes for a neutron entrance channel $c = n$. We assume that the only open channels are elastic scattering and neutron capture, $\Gamma_\lambda = \Gamma = \Gamma_n + \Gamma_\gamma$.

A series expansion of the trigoniometric factors gives for $\ell = 0$ at low energy in good approximation $\sin\phi_c = \rho = ka_c$ and $\sin\phi_c = 0$ for $\ell > 0$. The cosine term can be approximated by $\cos\phi_c = 1$ for all ℓ.

In the same way, the reaction cross section is

$$\sigma_{cc'} = \pi\lambda\!\!\!^{-2}_c g_c \frac{\Gamma_{\lambda c}\Gamma_{\lambda c'}}{(E - E_\lambda - \Delta_\lambda)^2 + \Gamma_\lambda^2/4} \tag{81}$$

and the shift Δ_λ results from the boundary condition.

2.3.2 The Breit-Wigner multi level approximation

Several resonances can be taken into account as a sum of Breit and Wigner single level cross sections. This is the most simple treatment of cross sections of many resonances. It neglects any possible interference between channels and levels (resonances).

The Breit and Wigner multi level (BWML) approach uses a sum over the levels in the collision matrix. In the inverse of the level matrix $\mathbf{A}$ all off-diagonal elements $A^{-1}_{\lambda\mu}$ are neglected, which means neglecting all interference terms between channels, but not between levels:

$$\left(\mathbf{A}^{-1}\right)_{\lambda\mu} = (E_\lambda - E + \Delta_\lambda - i\Gamma_\lambda/2)\delta_{\lambda\mu}, \tag{82}$$

$$U_{cc'} = e^{-i(\phi_c+\phi_{c'})}\left(\delta_{cc'} + \sum_\lambda \frac{i\sqrt{\Gamma_{\lambda c}\Gamma_{\mu c'}}}{E_\lambda + \Delta_\lambda - E - i\Gamma_\lambda/2}\right). \tag{83}$$

2.3.3 The Reich-Moore approximation

In the approximation of Reich and Moore [49] it is assumed that the amplitudes $\gamma_{\lambda c}$ are uncorrelated and have a Gaussian distribution with zero mean. This is a consequence of the chaotic behaviour of the compound nucleus, except for the very light nuclei. This is known as the Gaussian Orthogonal Ensemble [33, 52, 53].

In medium and heavy nuclei, the number of photon channels is very large. And since the amplitudes are supposed to have a random distribution with zero mean, the expectation value of the product of two amplitudes is zero for $\lambda \neq \mu$, *i.e.* $\langle\gamma_{\lambda c}\gamma_{\mu c}\rangle = \gamma^2_{\lambda c}\delta_{\lambda\mu}$. Summing over the photon channels gives

$$\sum_{c\in\text{photon}} \gamma_{\lambda c}\gamma_{\mu c} = \sum_{c\in\text{photon}} \gamma^2_{\lambda c}\delta_{\lambda\mu} = \Gamma_{\lambda\gamma}\delta_{\lambda\mu}. \tag{84}$$

Therefore the general expression for $\mathbf{A}^{-1}$, eq. (72), can be simplified for the photon channels and becomes

$$\begin{aligned}\left(\mathbf{A}^{-1}\right)_{\lambda\mu} &= (E_\lambda - E)\delta_{\lambda\mu} - \sum_{c\in\text{photon}} \gamma_{\lambda c}\gamma_{\mu c}(L_c - B_c) - \sum_{c\notin\text{photon}} \gamma_{\lambda c}\gamma_{\mu c}(L_c - B_c)\\ &= (E_\lambda - E)\delta_{\lambda\mu} - \Gamma_{\lambda\gamma}(L_c - B_c)\delta_{\lambda\mu} - \sum_{c\notin\text{photon}} \gamma_{\lambda c}\gamma_{\mu c}(L_c - B_c)\\ &= (E_\lambda - E + \Delta_\lambda - i\Gamma_{\lambda\gamma}/2)\delta_{\lambda\mu} - \sum_{c\notin\text{photon}} \gamma_{\lambda c}\gamma_{\mu c}(L_c - B_c).\end{aligned} \tag{85}$$

Comparing this to eq. (72), the approximation may be written as a reduced R-matrix in the sense that the photon channels are excluded and the eigenvalue E_λ is replaced by $E_\lambda - i\Gamma_{\lambda\gamma}/2$. This Reich-Moore R-matrix is

$$R_{cc'} = \sum_\lambda \frac{\gamma_{\lambda c}\gamma_{\lambda c'}}{E_\lambda - E - i\Gamma_{\lambda\gamma}/2} \quad c \notin \text{photon}. \tag{86}$$

The number of energy levels, which may be over hundreds of thousands in heavy nuclei, determines the number of possible photon decay channels. Excluding them reduces largely the number of channels and therefore the matrix inversion needed in the relation between the R-matrix and the cross sections. In the often occurring case at low energy that only the elastic scattering and neutron capture channels are open, the number of channels in the R-matrix is one, namely that of the neutron channel, the photon channels being excluded explicitly. The total radiation width is present however in the denominator of eq. (86). The R-matrix becomes in this case an R-function of which the inversion is trivial. Including other channels, like one or two fission channels, keeps the number of channels low and makes the inversion still feasible. This approximation of the general R-matrix is the most accurate one used.

2.4 Average cross sections

At higher energies the widths of the resonances overlap and the cross sections appear smooth and with a slow variation with energy. The total and scattering cross sections without sharply separated or observed resonances can be adequately described by representing the particle-nucleus interaction by a complex potential. This optical potential, so called because mathematically analogous to the scattering and absorption of light in a medium (cloudy crystal ball), results

in the partial scattering or absorption of the beam. The solution of the Schrödinger equation, usually numerically, with a given potential gives the wave functions from which the cross sections can be obtained [54]. Much progress has been made since in the theoretical development and parametrization of a suitable optical model potentials, see for example refs. [29, 55–59].

By making averages over resonances, the energy averaged collision matrix $\overline{U_{cc}}$ can be related to the energy-averaged cross sections $\overline{\sigma}$. The development of a given shape of the optical model potential results in a value for $\overline{U_{cc}}$. From the usual R-matrix expressions we can formulate a number of cross sections as follows. By analogy to eq. (47) the average scattering cross section $\overline{\sigma_{cc}}$ can be written as

$$\overline{\sigma_{cc}} = \pi \lambda\!\!\!^{-2}_c g_c \overline{|1 - U_{cc}|^2}, \tag{87}$$

which can be split up into an average shape elastic scattering cross section

$$\overline{\sigma^{\mathrm{se}}_{cc}} = \pi \lambda\!\!\!^{-2}_c g_c |1 - \overline{U_{cc}}|^2, \tag{88}$$

associated with potential scattering, and an average compound elastic scattering cross section due to resonance scattering

$$\overline{\sigma^{\mathrm{ce}}_{cc}} = \pi \lambda\!\!\!^{-2}_c g_c \left(\overline{|U_{cc}|^2} - |\overline{U_{cc}}|^2 \right) \tag{89}$$

and, after eq. (48), the average reaction cross section $\overline{\sigma_{cr}}$, corresponding to all non-elastic partial cross sections, as

$$\overline{\sigma_{cr}} = \pi \lambda\!\!\!^{-2}_c g_c (1 - \overline{|U_{cc}|^2}) \tag{90}$$

and, following eq. (49), the average total cross section $\overline{\sigma_{c,T}}$ can be written as

$$\overline{\sigma_{c,T}} = 2\pi \lambda\!\!\!^{-2}_c g_c (1 - \mathrm{Re}\, \overline{U_{cc}}). \tag{91}$$

The sum of the average compound elastic scattering cross section $\overline{\sigma^{\mathrm{ce}}_{cc}}$ and the average reaction cross section $\overline{\sigma_{cr}}$ can be considered as the cross section for the formation of the compound nucleus $\overline{\sigma_c}$, and can be written as

$$\begin{aligned} \overline{\sigma_c} = \overline{\sigma^{\mathrm{ce}}_{cc}} + \overline{\sigma_{cr}} &= \pi \lambda\!\!\!^{-2}_c g_c \left(\overline{|U_{cc}|^2} - |\overline{U_{cc}}|^2 + 1 - \overline{|U_{cc}|^2} \right) \\ &= \pi \lambda\!\!\!^{-2}_c g_c (1 - |\overline{U_{cc}}|^2). \end{aligned} \tag{92}$$

Then the sum of this compound nucleus formation cross section $\overline{\sigma_c}$ and the average shape elastic scattering cross section $\overline{\sigma^{\mathrm{se}}_{cc}}$ equals the total cross section $\overline{\sigma_{c,T}}$, which can be verified by

$$\begin{aligned} \overline{\sigma_c} + \overline{\sigma^{\mathrm{se}}_{cc}} &= \pi \lambda\!\!\!^{-2}_c g_c \left(1 - |\overline{U_{cc}}|^2 + |1 - \overline{U_{cc}}|^2 \right) \\ &= \pi \lambda\!\!\!^{-2}_c g_c \left(1 - |\overline{U_{cc}}|^2 + 1 - 2\,\mathrm{Re}\, \overline{U_{cc}} + |\overline{U_{cc}}|^2 \right) = \overline{\sigma_{c,T}}. \end{aligned} \tag{93}$$

From the above expressions, only the total, shape elastic, and compound nucleus formation cross sections $\overline{\sigma_{c,T}}$ $\overline{\sigma^{\mathrm{se}}_{cc}}$, and $\overline{\sigma_c}$ contain the elements $\overline{U_{cc}}$, calculated by optical model, without other terms like $\overline{|U_{cc}|^2}$ which cannot be extracted from optical model calculations. For a direct comparison with experimental data, only the calculated average total cross section (eq. (91)) can be used in a general way. The shape elastic scattering cross section cannot be distinguished from the compound elastic scattering. The calculated compound nucleus formation cross section (eq. (92)) is also not directly observable, but can be used in combination with measured decay channels, like in the surrogate measurements.

Finally the average cross section for a single reaction $\overline{\sigma_{cc'}}$ is

$$\overline{\sigma_{cc'}} = \pi \lambda\!\!\!^{-2}_c g_c \overline{|\delta_{cc'} - U_{cc'}|^2}, \tag{94}$$

which contains the nearly impossible averaging over $|U_{cc'}|^2$.

When we introduce the transmission coefficient

$$T_c = 1 - |U_{cc}|^2, \tag{95}$$

the compound nucleus formation cross section (unaveraged) can be written as

$$\sigma_c = \pi \lambda\!\!\!^{-2}_c g_c T_c. \tag{96}$$

Using the usual concepts in nuclear reaction theory (reciprocity, time-reversal invariance), the probability of decay through channel c' as $T_{c'}/\Sigma T_i$ the cross section for the reaction $c \to c'$ is then

$$\sigma_{cc'} = \pi \lambda\!\!\!^{-2}_c g_c T_c \frac{T_{c'}}{\Sigma T_i}\,, \tag{97}$$

where the sum runs over all possible channels. Averaging over a small energy interval with many resonances, taking into account shape elastic scattering in addition to compound reactions and redefining T_c as

$$T_c = 1 - |\overline{U_{cc}}|^2 \tag{98}$$

results in the Hauser-Feshbach formula (see also [34, 60–67] for more details)

$$\overline{\sigma_{cc'}} = \overline{\sigma^{\mathrm{se}}_{cc}}\delta_{cc'} + \pi\lambda\!\!\!^{-2}_c g_c \frac{T_c T_{c'}}{\Sigma T_i} W_{cc'}, \tag{99}$$

where the factor $W_{cc'}$ is factor which includes elastic enhancement and a correction for width fluctuations, which can be written as (see, for example, ref. [65])

$$W_{cc'} = \overline{\left(\frac{\Gamma_c \Gamma_{c'}}{\Gamma}\right)} \frac{\overline{\Gamma}}{\overline{\Gamma_c}\,\overline{\Gamma_{c'}}}\,. \tag{100}$$

The width fluctuations can be calculated most accurately using the GOE triple integral [68, 69], but also with simpler approximations.

The transmission coefficients for particle channels are given by eq. (98). Two other channels exist which are the photon and fission channels. Their transmission coefficients, related to the average widths $\overline{\Gamma_\gamma}$ and level spacing D, are defined as

$$T_\gamma = 2\pi \frac{\overline{\Gamma_\gamma}}{D} \tag{101}$$

and

$$T_f = 2\pi \frac{\overline{\Gamma_f}}{D}\,. \tag{102}$$

Dedicated modelizations on photon strength functions, level densities and fission models, are used for the photon and fission transmission coefficients, but are beyond the scope of this overview. Good starting points for further reading are the user guides of specialized computer codes like EMPIRE [70], TALYS [71], and others.

3 Level statistics from resolved resonances

3.1 Observables from resolved resonances

The nuclear unbound states immediately above the neutron binding energy are observed in neutron-induced reactions as resolved resonances. These resonances are characterized by their resonance parameters, which are the level energies $E_{\lambda,c}$ and the reduced amplitudes $\gamma_{\lambda,c}$, for a level λ and a channel c.

From experimental data of resolved resonances measured with the time-of-flight technique, the compound nucleus observables are the level energies E with spin and parities J^π and orbital momentum ℓ, and the different partial widths Γ_r summing up to the total width Γ. Depending on which reaction channels are open, the partial widths are the neutron width Γ_n, and for example the radiative width Γ_γ, the fission width Γ_f, or alpha width Γ_α. For neutron-induced reactions in the unresolved resonance region, average cross sections are usually extracted from the measured reaction yield and can be modelled with averages of these quantities.

One reason to parametrize neutron-induced cross sections in the resolved resonance region is to be able to reconstitute Doppler broadened cross sections, which are of practical use in neutron-rich environments, at any desired temperature, using only a limited number of physical quantities, the resonance parameters. An other important reason to obtain resonance parameters is to extract the average parameters. The statistical properties of the resonance parameters are important to deduce quantities which can be used to describe average cross sections and to quantify their fluctuations in the unresolved resonance region. Such parameters are the average level spacing $\langle D_\ell \rangle$, the average reduced neutron widths $\langle \Gamma^\ell_n \rangle$ and other average partial widths used in transmission coefficients as in eq. (101) and (102), and the related neutron strength functions $\langle S_\ell \rangle$ for a partial wave ℓ as defined in eq. (103). The neutron strength functions can be compared with results from optical model calculations [72–74]. While these quantities usually have only a slow energy dependence, they can be considered constant in the small window of excitation energies just above the neutron binding energy where resolved resonances can be observed. The neutron strength function S_ℓ is related to the quantities $\langle D_\ell \rangle$ and $\langle \Gamma^\ell_n \rangle$, which are inherent parameters of the underlying distributions, as

$$S_\ell = \frac{\langle \Gamma^\ell_n \rangle}{(2\ell+1) D_\ell}\,, \tag{103}$$

for which estimates have to be found based on observed resonance data. The reduced neutron width Γ_n^ℓ is for experimental data usually defined by

$$\Gamma_n^\ell = \frac{1}{v_\ell}\sqrt{\frac{1\,\mathrm{eV}}{E}}\Gamma_n, \tag{104}$$

with $v_0 = 1$, and

$$v^\ell = \frac{P_\ell}{P_0}\,, \tag{105}$$

with Γ_n the observable neutron width. This removes the energy dependence of the neutron width scaled at the arbitrary energy of 1 eV. Expressions for the penetrability factor P_ℓ are given in table 3, where in the R-matrix formalism, the channel width is related to the channel amplitude by $\Gamma_c = 2P_\ell\gamma_c^2$.

We will now focus on the estimates for $\langle D_\ell\rangle$, $\langle\Gamma_n^\ell\rangle$, and S_ℓ after a brief sketch of the historical development of random matrix theory related to neutron-induced reactions.

3.2 Random matrix theory

The nuclear states above the neutron separation energy, the resonances, are for most nuclei extremely complicated configurations of many-particle many-hole states. The stochastic behaviour of resolved compound nucleus resonances has been observed for neutron-induced, but also for proton-induced reactions near the Coulomb barrier, in many cases. In the early 1950s Wigner searched a description of the behaviour of the properties of energy levels and widths of the highly excited states observed in nuclear reactions with heavy nuclei [75]. Such a complex quantum system can be regarded as governed by a Hamiltonian represented by a large dimension Hermitian matrix. The development of random matrix theory was outlined in a series of papers by Wigner, Dyson and Mehta [76–82]. Random matrix theory gained more interest in the 1980s with the study of the field of quantum chaos, see for example ref. [83]. Nowadays random matrix theory has applications in many other fields like atomic physics and in various other non-nuclear or non-atomic complex systems showing chaotic behaviour. Extensive reviews on random matrices in nuclear physics can be found in refs. [84–86]. In many experimental nuclear data sets confirmation was found with the theoretical predictions [87, 88]. While several Gaussian ensembles were studied (GUE, GSE) one class of random matrices, the Gaussian Orthogonal Ensemble (GOE) was very successful in describing the statistical properties of nuclear energy levels of atomic nuclei. It results in particular distributions, both for the level widths, following a Porter-Thomas distribution (a chi-square distribution with one degree of freedom) [89] and for the level spacings, closely following a Wigner distribution [90].

3.3 The Porter-Thomas distribution of reaction widths

In same period, the first data on neutron-induced reactions were collected for many resonances in medium and heavy-mass nuclei at low neutron energy. By removing the energy dependence at the resonance energy E_r from the s-wave neutrons widths Γ_n, the reduced neutron widths $\Gamma_n^0 = \Gamma_n/\sqrt{E_r}$ are obtained. The values of Γ_n^0 were observed to show large fluctuations from one resonance to another in the same nucleus. Porter and Thomas [89] explained the fluctuations in terms of a Gaussian distribution of the reduced-width amplitudes, resulting in a chi-square distribution for the reduced neutron width observable, which is the square of the reduced-width amplitude. The dimensionless quantity,

$$x = \frac{\gamma_c^2}{\langle\gamma_c^2\rangle} = \frac{\Gamma_c^\ell}{\langle\Gamma_c^\ell\rangle}\,, \tag{106}$$

has the chi-square distribution with one degree of freedom, also called the Porter-Thomas distribution. The quantities x and γ_c are implicitly taken only for resonances of a given value of ℓ,

$$P_{\mathrm{PT}}(x) = \frac{1}{\sqrt{2\pi x}}\exp\left(-\frac{x}{2}\right), \tag{107}$$

or written as a probability density of Γ_c^ℓ

$$P_{\mathrm{PT},\Gamma}(\Gamma_c^\ell) = \sqrt{\frac{\Gamma_c^\ell}{2\pi\langle\Gamma_c^\ell\rangle}}\exp\left(-\frac{1}{2}\frac{\Gamma_c^\ell}{\langle\Gamma_c^\ell\rangle}\right), \tag{108}$$

which has a single parameter $\langle\Gamma_c^\ell\rangle$.

A plausible explanation for this was given by the nature of the reduced-width amplitude which is proportional to the matrix element of the state of the wave function of the compound nucleus and the wave function for the neutron channel. The rapidly oscillating internal wave function has many positive and negative contributions resulting in a zero expectation value of the matrix element and a random amplitude. Assuming a Gaussian distribution for γ_c seems reasonable and results in the Porter-Thomas distribution for the observable neutron widths.

This is also the basis of the statistical model of the nucleus which applies for many nuclei at high excitation energies, in particular for compound nuclei of medium and heavy-mass nuclei. The statistical behaviour also explains that it is impossible, at least in the near future, to predict energy positions and widths of levels at an excitation energy of roughly 10 MeV with a precision of better than 1 eV. This information is needed to calculate the fluctuating cross sections at low energy.

As stated, the reduced channel widths Γ_c^ℓ are related to a chi-square distribution with one degree of freedom $\nu = 1$ for a single channel c. Not all neutron widths correspond to a single channel specified by ℓ and J. If the target spin is not zero, the s-wave resonances have two possible spins. While for heavy nuclei at low energy s-wave resonances are much stronger than higher partial wave resonances, the spin is usually unknown. The resulting distribution of the reduced widths corresponds therefore not to a chi-square distribution with $\nu = 1$ but with $\nu = 2$, assuming the same average width.

The same Porter-Thomas fluctuations are expected to be present in other observable widths. The radiative width is in fact the sum of many widths of gamma-ray transitions from the resonance state to lower-lying levels. While a single statistical gamma transition to a given level shows PT fluctuations from one resonance to another, the sum of many transitions resembles a chi-square distribution with a high number of degrees of freedom, and closely resembles a Gaussian. Indeed the radiation width, especially for heavy nuclei, is rather constant for many resonances.

Fission widths are a special case. Observed widths for fission follow a chi-square distribution with only a small, even fractional number of degrees of freedom. The many possible pairs of fission fragments in different excited states should not be considered as exit channels, but instead the few possible states available at the saddle point, just before fission. This results in an effective value of ν of about 3 or 4.

In order to estimate the average width from experimental data, we focus on a sequence of observed neutron widths $\Gamma_{n,i}$ from resonances with the same spin and orbital momentum. From experiments many data are available for s-wave resonances ($\ell = 0$) for even-even nuclei ($I = 0$, so $J = 1/2$). Using the Porter-Thomas distribution eq. (107) for $\Gamma_{n,i}^\ell$ which are considered independent, we construct the likelihood function and find its maximum by setting the second derivative of the log-likelihood function to zero. The maximum is found at the average of the values $\Gamma_{n,i}^\ell$. This estimator is unbiased and its expectation value equals $\langle \Gamma_c^\ell \rangle$. Using the likelihood function, the variance can be calculated as the expectation value of $(\Gamma_n^\ell - \langle \Gamma_c^\ell \rangle)^2$, giving the estimator $\hat{\Gamma}_n^\ell$ for $\langle \Gamma_n^\ell \rangle$ and its standard deviation $\mathrm{std}(\hat{\Gamma}_n^\ell)$ [91] as

$$\hat{\Gamma}_n^\ell = \frac{1}{N} \sum_i \Gamma_{n,i}^\ell, \tag{109}$$

$$\frac{\mathrm{std}(\hat{\Gamma}_n^\ell)}{\hat{\Gamma}_n^\ell} = \sqrt{\frac{2}{N}}\,. \tag{110}$$

This is only the variance of the estimator due to the distribution. Usually experimental uncertainties on $\Gamma_{n,i}^\ell$ have to be taken into account as well, separating the independent, uncorrelated uncertainties, and the correlated uncertainties like normalization that apply to all $\Gamma_{n,i}^\ell$.

The Porter-Thomas distribution can be used to estimate the number of levels missed in measurements, especially in estimation D_0 which is a crucial input and calibration parameter for level density models. Since the number of observed resonances are usually limited, binning the available widths will remove information. Instead, it is more convenient to work with unbinned data, for which the cumulative distribution function is more appropriate, or the complementary cumulative distribution function in the case of missing level estimation. For the Porter-Thomas distribution this is

$$C_{\mathrm{PT}}(x) = \int_x^\infty P_{\mathrm{PT}}(x')\mathrm{d}x' = 1 - \mathrm{erf}(x/2). \tag{111}$$

Using the value x as an observation threshold for experimental data allows to fit the Porter-Thomas distribution using those resonances with a Γ_n large enough to be detected in a measurement. The extrapolation to zero threshold gives then the expected number of resonances for the used interval of energy. Such a missing level correction is then used to obtain a correct value of D_0.

The Porter-Thomas distribution has been studied and verified for many data sets since a long time, see for example this study for a set of even-even nuclei (so with a single spin for $\ell = 0$ s-wave resonances) [92], but is still object of further studies [93, 94]. A fully statistical behaviour of the excited nucleus is of course a crude simplification. In particular for lighter nuclei and closed shell nuclei shell effects and other collective states play a major role. On the other hand, the statistical model works relatively well for medium and especially for heavy mass nuclei.

3.4 The Wigner distribution of level spacings

In the early days of random matrix theory, Wigner stated that the distribution of consecutive highly excited nuclear levels of a heavy nucleus follows a distribution known as the "Wigner's surmise",

$$P_{\mathrm{W}}(x) = \frac{\pi}{2} x \exp\left(-\frac{\pi}{4}x^2\right), \tag{112}$$

with x defined as

$$x = \frac{D}{\langle D\rangle} \tag{113}$$

and D is the next-neighbour or next-nearest-neighbour spacing $D = E_{\lambda+1} - E_\lambda$. Writing this explicitly for the level spacing gives

$$P_{\mathrm{W},D}(D) = \frac{\pi}{2}\frac{D}{\langle D\rangle^2}\exp\left(-\frac{\pi}{4}\frac{D^2}{\langle D\rangle^2}\right). \tag{114}$$

Note that this spacing is sometimes called nearest-neighbour spacing, which suggests a spacing $\min(E_{\lambda+1} - E_\lambda, E_\lambda - E_{\lambda-1})$ which is actually a different distribution.

Wigner's surmise is valid for 2×2 matrices. Also for larger matrices Mehta [90] and Gaudin [96] found distributions that were not exactly, but very close to the Wigner level spacing distribution. Because of the convenient compact form, the Wigner distribution is widely used for experimental data.

The Wigner distribution is in fact a special case of the Rayleigh distribution. An important characteristic of this distribution is that the probability for small values of x tends to zero. For nuclear levels this is also known as the level repulsion property, which is the vanishing probability that two levels of a same J, ℓ sequence overlap. Wigner illustrated this with the spacing of the eigenvalues of a random 2×2 real symmetric matrix. With the development of Gaussian Ensembles of random matrices, particular attention was given to the Gaussian Orthogonal Ensemble (GOE) in the frame of nuclear physics. Such a random matrix has independent matrix elements with a Gaussian distribution and is invariant under orthogonal transformations.

To find an estimate $\hat{D}_\ell$ for the level spacing $\langle D_\ell\rangle$ from individual observations $D_{\ell,i}$, we construct again the likelihood function, now using the distribution eq. (112), and find its maximum by setting the second derivative of the log-likelihood function to zero. The estimator that results from this is however biased, which means that the expectation value of $\hat{D}_\ell$ is not equal to $\langle D_\ell\rangle$. Taking the average level spacing as estimator gives an unbiased estimator for $\langle D_\ell\rangle$, with a variance equal to $(4-\pi)/\pi \approx 0.273$ [91]. Nevertheless this estimator does not take into account the correlation predicted by the GOE, and found in agreement with observations in experimental data [97]. Two adjacent level spacings are anti-correlated. This means that a large spacing is followed more likely by a small spacing and vice versa. For a 3×3 matrix Porter [98] found the exact correlation of $(8\pi - 27)/(11\pi - 27) \approx -0.253$. For larger matrices the correlation is approximately

$$\rho(D_\lambda, D_{\lambda+1}) = \frac{\mathrm{cov}(D_\lambda, D_{\lambda+1})}{\mathrm{std}(D_\lambda)\,\mathrm{std}(D_{\lambda+1})} \approx -0.27, \tag{115}$$

resulting in a well-observed spectral rigidity in the positions of the levels. Dyson and Mehta [81] suggested that the number of observed levels N in an energy interval ΔE was a sufficient statistic for $\langle D_\ell\rangle$ and found the corresponding variance. The estimators are then

$$\hat{D}_\ell = \frac{\Delta E}{N}, \tag{116}$$

$$\frac{\mathrm{std}(\hat{D}_\ell)}{\hat{D}_\ell} = \frac{2}{\pi^2}\left(\ln(2\pi N) + 1 + \gamma - \frac{\pi^2}{8}\right)\Big/ N \approx \frac{0.45\sqrt{\ln(N)+2.18}}{N}, \tag{117}$$

where γ stands for the Euler constant (not an amplitude). The expression for this variance, used by ref. [99], is only very slowly diverging from $1/N$, and considerably larger than the $(4-\pi)/\pi/N$ from the maximum likelihood estimator. But the main issue with estimating $\langle D_\ell\rangle$ is related to the spurious and missing levels in the sequence to be analysed, which has a direct impact on the neutron strength function.

3.5 The neutron strength function

Liou and Rainwater [100] reviewed previous work on the practical application of estimating the neutron strength function [91, 101]. With the definition of eq. (103) and using the estimates eq. (116) and eq. (109), the widely used estimator for the strength function becomes

$$\hat{S}_\ell = \frac{\hat{\Gamma}_n^\ell}{(2\ell+1)\hat{D}_\ell} = \frac{\sum_i \Gamma_{n,i}^\ell}{(2\ell+1)}\Delta E. \tag{118}$$

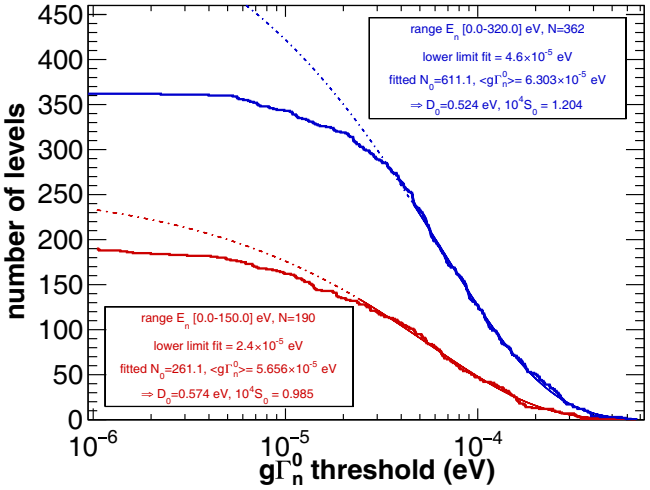

Fig. 7. The use of the Porter-Thomas distribution to estimate the same level spacing D_0 from a sequence of resonances in two different energy intervals, indicated in red and blue. For each interval, the experimental data is shown together with the expected complementary cumulative distribution. The range above the threshold used in the fit is shown as a solid line, while the remainder of the curve is shown as a dashed line. Taken from [95].

The aforementioned estimates can be applied only to a complete and pure sequence of levels of the same J and ℓ. The closest approach for such a sequence comes from s-wave resonances, so for $\ell = 0$. Since higher partial waves become only significant at higher incident neutron energies, it is extremely difficult to have usable sequences for $\ell > 1$, while for p-waves ($\ell = 1$) the information is always limited.

Favourable nuclei for pure s-wave sequences are the heavy mass nuclei in the $150 < A < 190$ range where the S_0 strength function shows a maximum. For the even-even nuclei, since they have spin $I = 0$, the compound nucleus s-wave resonances ($\ell = 0$) have all spin-parity $J = 1/2^+$, while resonances from higher partial waves are very unlikely. Getting precise values for the resonance parameters can then be achieved from spectroscopy of neutron resonances measured both in capture and transmission experiments with samples of several thicknesses. Early examples for such data are the series of measurements using enriched isotopes of Cd [102], Er [103], W [104], Yb [105], Dy [106].

For spin $I \neq 0$ target nuclei, two s-wave spins $I \pm 1/2$ are possible. Since in addition the spin is usually not known, usually the quantity $g\Gamma_n^\ell$ is used instead of Γ_n^ℓ in all previous estimations. Missing levels in a sequence are presumably unobserved because of their small value of Γ_n^ℓ and do therefore not substantially influence the sum in eq. (118). For medium and heavy mass nuclei, spurious levels from higher partial waves also have smaller values of Γ_n^ℓ. For nuclei with a more sizeable influence of p-waves in the resolved resonance region, but still with a negligible contribution from d-waves and higher partial waves, Bollinger and Thomas [107] used an approach based on the magnitude of the neutron widths depending on the large difference in the penetrability factor for s and p-waves. Liou and Rainwater [100] suggest the use of probability tables based on Monte Carlo simulations.

The average level density however is much more sensitive to missing and spurious levels. While the mixture of sequences has been addressed theoretically in ref. [81], the practical application to measured data is not straightforward. Counting of levels in an interval ΔE as is done in eq. (118) is insufficient and corrections for missing levels must be applied.

One approach to account for missing levels in the level spacing is the "staircase" method where the cumulated number of levels is plotted against energy. Since the level density is constant in the energy range under consideration, we expect a straight line. Usually at higher energies it is more likely to miss levels and only the energy interval of the linear part is then used to count levels. This is also the basis of the so-called Δ_3 statistic [81] which is the mean square deviation of the cumulative number of resonances as a function of energy from a straight line fit. The Δ_3 statistic does however not account for admixtures of other sequences or the fact that the missing fraction of levels may be linear with energy.

In recent work, the following procedure has been used. First a prior separation of s and p-waves, based on the method described in ref. [107], was applied. The in this way obtained s-wave sequence was then compared to the cumulative Porter-Thomas distribution eq. (111) to adjust the free parameter, the number of levels that should have been observed, from the resonances with large values of Γ_n. This was applied in for example, the nuclei ^{99}Tc [108], ^{232}Th [109], ^{241}Am [95] (see the example in fig. 7) or ^{242}Pu [110].

To illustrate the previously discussed points, we show in fig. 8 the level sequences for the nuclei ^{27}Al, ^{56}Fe, ^{197}Au and ^{238}U, as extracted from evaluated nuclear data libraries. For each nucleus, on the left side the neutron width is plotted as a function of the position of the resonances for a given $J, \ell = 0$ sequence. On the middle panels the distributions of the level spacing are shown, while on the right panels the Porter-Thomas distributions are shown.

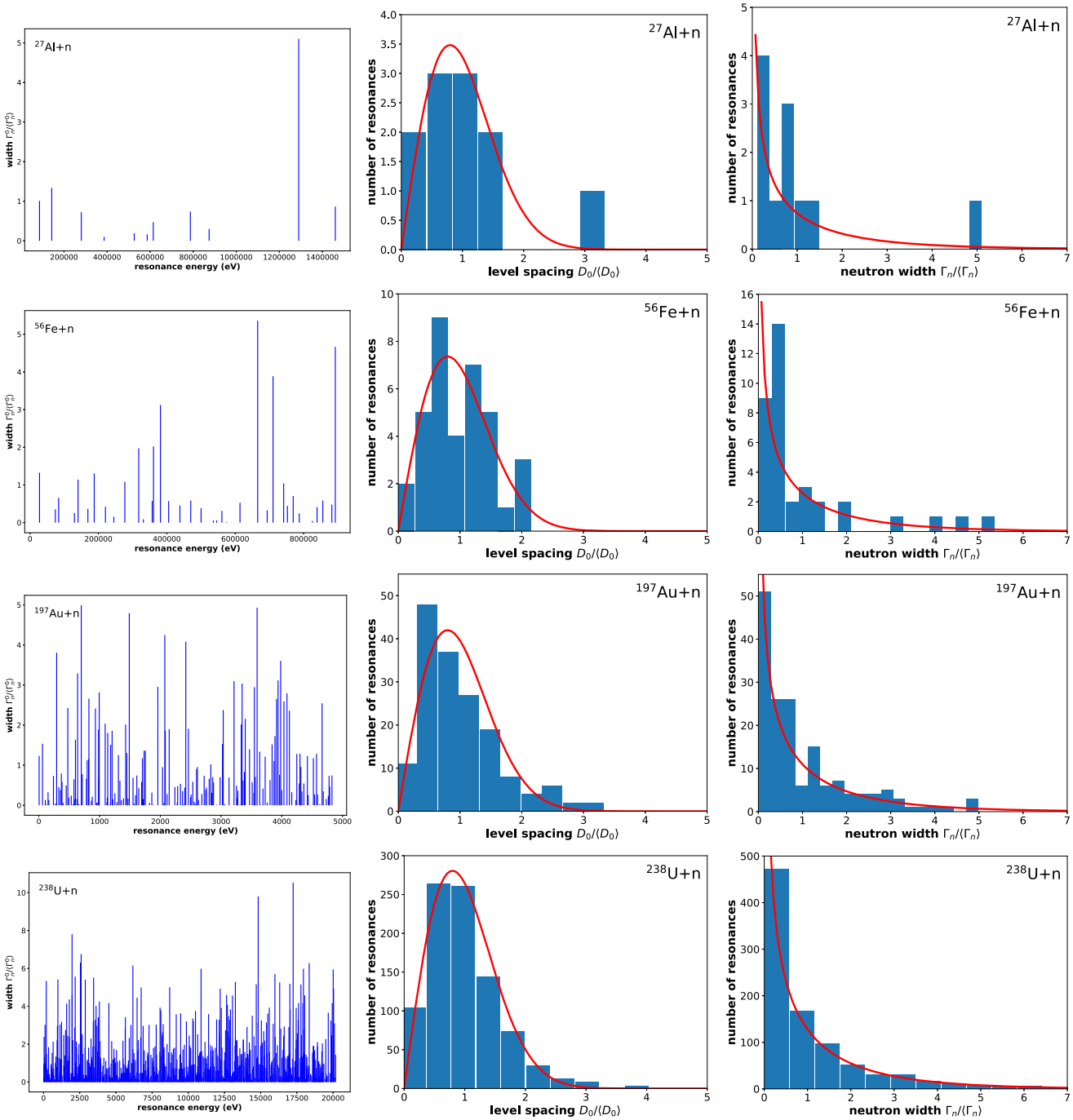

Fig. 8. For the nuclei ^{27}Al, ^{56}Fe, ^{197}Au and ^{238}U, the position of resonances *versus* their normalized reduced neutron width is shown in on the left side. In the middle figures the distribution of the spacing between successive levels is shown as a histogram together with the expected distribution from eq. (112), scaled to the histogram. In the right figures a histogram of the normalized reduced neutron width is shown together with the scaled expected Porter-Thomas distribution. For each of the four nuclei only resonances of a single sequence with the same orbital momentum ($\ell = 0$) and with the same spin ($J = 3$, 1/2, 2, and 1/2 for a number of 11, 36, 164 and 903 resonances, respectively) were taken.

The advantage of using an evaluated library is that the included information is complete, the disadvantage that it is not necessarily correct for the purpose of exploiting level statistics. For example spins and orbital momenta are usually not known. Depending on the evaluation, they may have been assigned taking into account the corresponding probability distributions. This is a necessary step in having complete information for every levels. To be sure that only experimentally observed levels are used it can be more prudent to use a data compilation like ref. [111].

4 Concluding remarks

The importance of neutron-induced reaction data is evident in a wide variety of research fields, ranging from stellar nucleosynthesis and nuclear structure to applications of nuclear technology. For this purpose, neutron beams from accelerators, including recently constructed and upcoming facilities, are significant suppliers of nuclear data [28]. Resonances in the reaction cross sections are an important feature and need to be quantified using the R-matrix formalism which links measurable nuclear properties to useable nuclear cross sections. The statistical properties of the resonance parameters give access to neutron strength functions and level density information, needed for cross section calculations at higher energies, and for systematics trends on the chart of nuclei. The provided references form a good starting point for a more complete picture of this field.

References

1. N. Bohr, Nature **137**, 344 (1936).
2. J.R. Santisteban, L. Edwards, H.G. Priesmeyer *et al.*, Appl. Phys. A **74**, s1616 (2002).
3. R.A. Alpher, H. Bethe, G. Gamow, Phys. Rev. **73**, 803 (1948).
4. E. Margaret Burbidge, G.R. Burbidge, William A. Fowler *et al.*, Rev. Mod. Phys. **29**, 547 (1957).
5. George Wallerstein, Icko Iben, Peter Parker *et al.*, Rev. Mod. Phys. **69**, 995 (1997).
6. F. Käppeler, R. Gallino, S. Bisterzo *et al.*, Rev. Mod. Phys. **83**, 157 (2011).
7. S.E. Woosley, A. Heger, T.A. Weaver, Rev. Mod. Phys. **74**, 1015 (2002).
8. Stephane Goriely, Andreas Bauswein, Hans-Thomas Janka, Astrophys. J. **738**, L32 (2011).
9. Claude Bloch, Phys. Rev. **93**, 1094 (1954).
10. Torleif Ericson, Adv. Phys. **9**, 425 (1960).
11. J.R. Huizenga, L.G. Moretto, Annu. Rev. Nucl. Sci. **22**, 427 (1972).
12. A.S. Iljinov, M.V. Mebel, N. Bianchi *et al.*, Nucl. Phys. A **543**, 517 (1992).
13. Till von Egidy, Dorel Bucurescu, Phys. Rev. C **72**, 044311 (2005).
14. H. Nakamura, T. Fukahori, Phys. Rev. C **72**, 064329 (2005).
15. S. Goriely, S. Hilaire, A.J. Koning, Phys. Rev. C **78**, 064307 (2008).
16. S.M. Qaim, J. Radioanal. Nucl. Chem. **305**, 233 (2015).
17. G. Aliberti *et al.*, Nucl. Sci. Eng. **146**, 13 (2004).
18. A. Nuttin *et al.*, Ann. Nucl. Energy **40**, 171 (2012).
19. H. Brysk, Plasma Phys. Controlled Fusion **15**, 611 (1973).
20. J. Eriksson *et al.*, Comput. Phys. Commun. **199**, 40 (2016).
21. A.J. Koning *et al.*, J. Korean Phys. Soc. **59**, 1057 (2011).
22. M.B. Chadwick *et al.*, Nucl. Data Sheets **112**, 2887 (2011).
23. K. Shibata, J. Nucl. Sci. Technol. **50**, 449 (2013).
24. A.M. Lane *et al.*, Rev. Mod. Phys. **30**, 257 (1958).
25. W.E. Lamb, Phys. Rev. **55**, 190 (1939).
26. I. Dillmann *et al.*, *KADoNiS v0.3*, `http://www.kadonis.org` (2009).
27. N. Otuka *et al.*, Nucl. Data Sheets **120**, 272 (2014).
28. N. Colonna, F. Gunsing, F. Käppeler, Prog. Part. Nucl. Phys. **101**, 177 (2018).
29. E. Bauge, J.P. Delaroche, M. Giro, Phys. Rev. C **63**, 024607 (2001).
30. G.L. Payne, L. Schlessinger, Phys. Rev. C **2**, 1648 (1970).
31. R. Shyam, O. Scholten, Phys. Rev. C **78**, 065201 (2008).
32. E.P. Wigner, L. Eisenbud, Phys. Rev. **72**, 29 (1947).
33. J.E. Lynn, *The Theory of Neutron Resonance Reactions* (Clarendon Press, Oxford, 1968).
34. F. Fröhner, Tech. rep. JEFF Report 18, OECD/NEA (2000).
35. P. Descouvemont, D. Baye, Rep. Prog. Phys. **73**, 036301 (2010).
36. J. Humblet, L. Rosenfeld, Nucl. Phys. **26**, 529 (1961).
37. E. Vogt, Rev. Mod. Phys. **34**, 723 (1962).
38. F. Schmittroth, W. Tobocman, Phys. Rev. C **3**, 1010 (1971).
39. D.B. Adler, F.T. Adler, Phys. Rev. C **6**, 986 (1972).
40. C. Chandler, W. Tobocman, Phys. Rev. C **19**, 1660 (1979).
41. T.A. Brody, J. Flores, J.B. French *et al.*, Rev. Mod. Phys. **53**, 385 (1981).
42. J. Humblet, Phys. Rev. C **42**, 1582 (1990).
43. H. Feshbach, *Theoretical Nuclear Physics; Nuclear Reactions* (John Wiley & Sons, 1991).
44. A.A. Luk'yanov, N.B. Yaneva, Phys. Part. Nucl. **28**, 331 (1997).
45. C.R. Brune, Phys. Rev. C **66**, 044611 (2002).
46. M. Abramowitz, *Handbook of Mathematical Functions with Formulas, Graphs, and Mathematical Tables* (Dover Publications, New York, 1965).
47. D. Zwillinger, *CRC Standard Mathematical Tables and Formulae* (CRC Press, 2003).

48. J.M. Blatt, L.C. Biedenharn, Rev. Mod. Phys. **24**, 258 (1952).
49. C.W. Reich, M.S. Moore, Phys. Rev. **111**, 929 (1958).
50. P.L. Kapur, R.E. Peierls, Proc. R. Soc. A **166**, 277 (1938).
51. R.N. Hwang, Nucl. Sci. Eng. **52**, 157 (1973).
52. M.L. Mehta, Nucl. Phys. **18**, 395 (1960).
53. M.L. Mehta, *Random Matrices* (Academic Press, 1991).
54. S. Fernbach, R. Serber, T.B. Taylor, Phys. Rev. **75**, 1352 (1949).
55. H.S. Camarda, F.S. Dietrich, T.W. Phillips, Phys. Rev. C **39**, 1725 (1989).
56. H. Leeb, S. Wilmsen, Phys. Rev. C **62**, 024602 (2000).
57. F.S. Dietrich, J.D. Anderson, R.W. Bauer *et al.*, Phys. Rev. C **67**, 041301(R) (2003).
58. R. Capote, E.S. Soukhovitskii, J.M. Quesada *et al.*, Phys. Rev. C **72**, 064610 (2005).
59. J.M. Quesada, R. Capote, E.S. Soukhovitskii *et al.*, Phys. Rev. C **76**, 057602 (2007).
60. W. Hauser, H. Feshbach, Phys. Rev. **87**, 366 (1952).
61. H. Feshbach, C.E. Porter, V.F. Weisskopf, Phys. Rev. **96**, 448 (1954).
62. P.E. Hodgson, *Nuclear Reactions and Nuclear Structure* (Clarendon Press, Oxford, 1971).
63. P.A. Moldauer, Phys. Rev. C **11**, 426 (1975).
64. P.A. Moldauer, Phys. Rev. C **12**, 744 (1975).
65. P.A. Moldauer, Phys. Rev. C **14**, 764 (1976).
66. P.A. Moldauer, Nucl. Phys. A **344**, 185 (1980).
67. I. Sirakov, R. Capote, F. Gunsing *et al.*, Ann. Nucl. Energy **35**, 1223 (2008).
68. J.J.M. Verbaarschot, H.A. Weidenmuller, M.R. Zirnbauer, Phys. Rep. **129**, 367 (1985).
69. J.J.M. Verbaarschot, Ann. Phys. **168**, 368 (1986).
70. M. Herman, R. Capote, B.V. Carlson *et al.*, Nucl. Data Sheets **108**, 2655 (2007).
71. A.J. Koning, S. Hilaire, M. Duijvestijn, Technical report (2007).
72. H. Feshbach, C.E. Porter, V.F. Weisskopf, Phys. Rev. **96**, 448 (1954).
73. G.E. Brown, Rev. Mod. Phys. **31**, 893 (1959).
74. P.E. Hodgson, Rep. Prog. Phys. **34**, 765 (1971).
75. E.P. Wigner, Ann. Math. **62**, 548 (1955).
76. E.P. Wigner, Ann. Math. **65**, 203 (1957).
77. E.P. Wigner, Ann. Math. **67**, 325 (1958).
78. F.J. Dyson, J. Math. Phys. **3**, 140 (1962).
79. F.J. Dyson, J. Math. Phys. **3**, 157 (1962).
80. F.J. Dyson, J. Math. Phys. **3**, 166 (1962).
81. F.J. Dyson, M.L. Mehta, J. Math. Phys. **4**, 701 (1963).
82. M.L. Mehta, F.J. Dyson, J. Math. Phys. **4**, 713 (1963).
83. O. Bohigas, M.J. Giannoni, C. Schmit, Phys. Rev. Lett. **52**, 1 (1984).
84. T.A. Brody, J. Flores, J.B. French *et al.*, Rev. Mod. Phys. **53**, 385 (1981).
85. H.A. Weidenmüller, G.E. Mitchell, Rev. Mod. Phys. **81**, 539 (2009).
86. G.E. Mitchell, A. Richter, H.A. Weidenmüller, Rev. Mod. Phys. **82**, 2845 (2010).
87. M. Carmeli, J. Stat. Phys. **10**, 259 (1974).
88. J.B. French, Nucl. Phys. A **396**, 87 (1983).
89. C.E. Porter, R.G. Thomas, Phys. Rev. **104**, 483 (1956).
90. M.L. Mehta, Nucl. Phys. **18**, 395 (1960).
91. D.D. Slavinskas, T.J. Kennett, Nucl. Phys. **85**, 641 (1966).
92. H.S. Camarda, Phys. Rev. C **49**, 1391 (1994).
93. A. Volya, H.A. Weidenmüller, Vladimir Zelevinsky, Phys. Rev. Lett. **115**, 052501 (2015).
94. V.V. Sokolov, Acta Phys. Pol. A **132**, 1704 (2017).
95. n_TOF Collaboration (K. Fraval *et al.*), Phys. Rev. C **89**, 044609 (2014).
96. M. Gaudin, Nucl. Phys. **25**, 447 (1961).
97. H.S. Camarda, P.D. Georgopulos, Phys. Rev. Lett. **50**, 492 (1983).
98. Charles E. Porter, Nucl. Phys. **40**, 167 (1963).
99. R. Capote, M. Herman, P. Obložinský *et al.*, Nucl. Data Sheets **110**, 3107 (2009).
100. H.I. Liou, J. Rainwater, Phys. Rev. C **6**, 435 (1972).
101. H.V. Muradyan, Yu.V. Adamchuk, Nucl. Phys. **68**, 549 (1965).
102. H.I. Liou, G. Hacken, F. Rahn *et al.*, Phys. Rev. C **10**, 709 (1974).
103. H.I. Liou, H.S. Camarda, S. Wynchank *et al.*, Phys. Rev. C **5**, 974 (1972).
104. H.S. Camarda, H.I. Liou, G. Hacken *et al.*, Phys. Rev. C **8**, 1813 (1973).
105. H.I. Liou, H.S. Camarda, G. Hacken *et al.*, Phys. Rev. C **7**, 823 (1973).
106. H.I. Liou, G. Hacken, J. Rainwater *et al.*, Phys. Rev. C **11**, 462 (1975).
107. L.M. Bollinger, G.E. Thomas, Phys. Rev. **171**, 1293 (1968).
108. F. Gunsing, A. Leprêtre, C. Mounier *et al.*, Phys. Rev. C **61**, 054608 (2000).
109. n_TOF Collaboration (F. Gunsing *et al.*), Phys. Rev. C **85**, 064601 (2012).
110. n_TOF Collaboration (J. Lerendegui-Marco *et al.*), Phys. Rev. C **97**, 024605 (2018).
111. S.I. Sukhoruchkin, Z.N. Soroko, V.V. Deriglazov, *Low Energy Neutron Physics - Tables of Neutron Resonance Parameters*, edited by H. Schopper (Springer, Landolt-Börnstein, 2004).